



HAL
open science

Evidence of mud volcanism due to the rapid compaction of Martian tsunami deposits in southeastern Acidalia Planitia, Mars

Ilaria Di Pietro, Antoine Séjourné, F. Costard, Marta Ciałzela, J. Alexis
Palmero Rodriguez

► To cite this version:

Ilaria Di Pietro, Antoine Séjourné, F. Costard, Marta Ciałzela, J. Alexis Palmero Rodriguez. Evidence of mud volcanism due to the rapid compaction of Martian tsunami deposits in southeastern Acidalia Planitia, Mars. *Icarus*, 2021, 354, pp.114096. 10.1016/j.icarus.2020.114096 . hal-02982488

HAL Id: hal-02982488

<https://cnrs.hal.science/hal-02982488v1>

Submitted on 3 Dec 2020

HAL is a multi-disciplinary open access archive for the deposit and dissemination of scientific research documents, whether they are published or not. The documents may come from teaching and research institutions in France or abroad, or from public or private research centers.

L'archive ouverte pluridisciplinaire **HAL**, est destinée au dépôt et à la diffusion de documents scientifiques de niveau recherche, publiés ou non, émanant des établissements d'enseignement et de recherche français ou étrangers, des laboratoires publics ou privés.

Evidence of mud volcanism due to the rapid compaction of Martian tsunami deposits in southeastern Acidalia Planitia, Mars

Ilaria Di Pietro^{a1}, Antoine Séjourné^b, François Costard^b, Marta Ciałzela^c and J. Alexis Palmero Rodriguez^d

^a International Research School of Planetary Sciences (IRSPS), Dipartimento di Ingegneria e Geologia (INGEO), Università degli Studi Gabriele d'Annunzio, viale Pindaro 42, 65127 Pescara, Italy

^b Géosciences Paris Sud (GEOPS), UMR 8148, Université Paris-Sud, CNRS, Rue du Belvédère, 91400 Orsay, France

^c Space Research Centre, Polish Academy of Sciences (PAS), ul. Bartycka 18A, 00-716 Warsaw, Poland

^d Planetary Science Institute (PSI), 1700 E Fort Lowell Rd # 106, 85719 Tucson, Arizona, USA


¹ Dipartimento di Scienze Psicologiche, della Salute e del Territorio (DISPUTER), Università degli Studi Gabriele d'Annunzio, via dei Vestini 32, 66100 Chieti, Italy

Corresponding author:

Ilaria Di Pietro

Dipartimento di Scienze Psicologiche, della Salute e del Territorio (DISPUTER),
Università degli Studi G. d'Annunzio, Via dei Vestini, 31 - 66100 Chieti, Italy

 ilaria.dipietro@unich.it

 +393275863091

Abstract

Thumbprint terrain was first recognized in Viking Orbiter data and described as sets of alternating continuous parallel ridges and depressions up to several tens of kilometres in length, with high and low albedo respectively. We performed a geomorphological analysis of these features using both Context Camera and High Resolution Imaging Science Experiment images, as well as topographic profiles based on Mars Orbiter Laser Altimeter data, with the aim to provide an origin for thumbprint terrain and constrain the geological evolution of southeastern Acidalia Planitia. The identification of runup lobate deposits, coupled with the putative presence of a Late Hesperian ocean in the northern lowlands, led to speculations that evidence of tsunamis may be present in the geologic record of the area. There are several hypotheses that have been proposed previously to explain the origin of thumbprint terrain and include ice-related, volcanic-related, liquefaction and mud-volcanism driven processes. However, a tsunami-related origin provides a strong geological framework for the energy required for the associated lobes to flow uphill and leaving peripheral termination ridges as a result of viscosity. Numerical simulations indicate that - prior to their emplacement - the lobes sustained high velocities, thereby lending further support to the tsunami hypothesis and their origin from the Lomonosov crater impact. Wave interference patterns, formed during the propagation of the tsunamis over and around prominent topography, likely explain the thumbprint terrain spatial arrangement. The thumbprint terrain sedimentary cones are, herein, considered mud volcanoes related to a tsunami that occurred in southeastern Acidalia Planitia.

1 Introduction

The presence of a Hesperian ocean within the northern plains is one of the most debated issues of the Martian geology (Parker et al., 1989, 1993; Head et al., 1998, 1999; Clifford and Parker, 2001; Carr and Head, 2003; Tanaka et al., 2003, 2005). Its presence would imply that northern lowlands gathered a large quantity of water and sediments. Outflow channels, carved by large-scale floods (Carr, 1979), are commonly thought to have served as the primary supply of water which may have filled the northern lowlands in the Late Hesperian (Parker et al., 1989, 1993; Baker et al., 1991; Clifford and Parker, 2001; Tanaka et al., 2005). The ocean-hypothesis is supported by several flat surfaces that can be observed spanning thousands of kilometres and marking distinct units in the peripheral northern lowlands. These limits have been interpreted as paleo-shorelines (Parker et al., 1989, 1993; Clifford and Parker, 2001); for example, the Deuteronilus contact is characterized by very slight topographic variations (-3792 ± 236 m), which are strikingly consistent with the paleo-shoreline hypothesis (Clifford and Parker, 2001; Carr and Head, 2003; Perron et al., 2007; Citron et al., 2018). On the other hand, some limits (i.e., Arabia contact) have topographic amplitudes of up to several kilometres that have initially been used against the ocean hypothesis (Head et al., 1998; Head et al., 1999; Carr and Head, 2003). However, recent studies proposed that these limits represent deformed paleo-shorelines as the result of deformation related to true polar wander occurring before and during the massive Tharsis volcanic rise (Citron et al., 2018; Zuber, 2018) or after the formation of Tharsis region (Perron et al., 2007). Several studies have also showed that there could be a large reservoir of water/mud in the deepest portions of the Utopia basin during the Hesperian (Ivanov et al., 2014; Ivanov et al., 2015). This may potentially represent the remnant of a larger standing body of water, further supporting the presence of an ocean within the northern plains (Parker et al., 1989, 1993; Head et al., 1998, 1999; Clifford and Parker, 2001; Carr and Head, 2003; Tanaka et al., 2003, 2005).

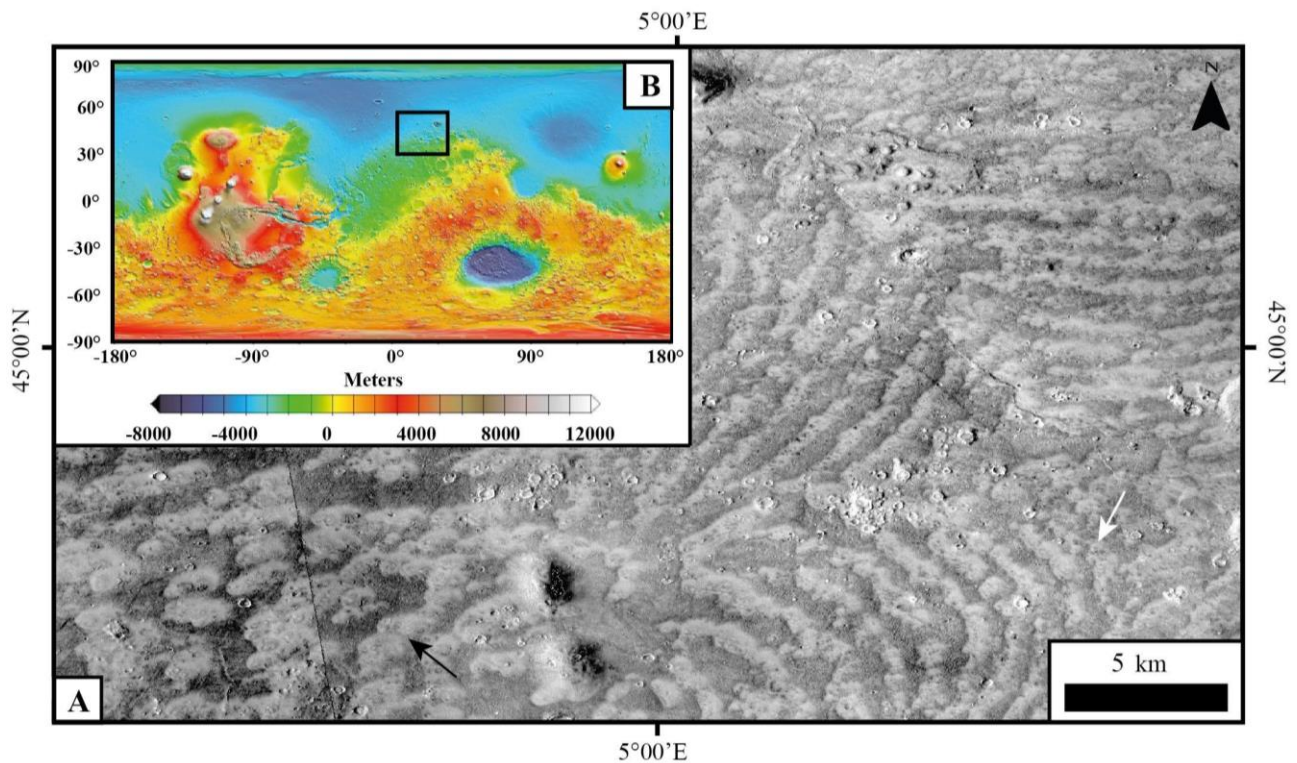


Figure 1. Thumbprint terrain in Acidalia Planitia. A) Thumbprint terrain at low resolution with a random arrangement (black arrow) on the left and an arcuate and parallel linear disposition (white arrow). B) Study area is marked by the black rectangle on the topographic map based on colorized Mars Orbiter Laser Altimeter data. Courtesy of NASA/JPL/Univ. of Arizona.

Thumbprint terrain (represented hereafter as TT) was previously recognized and described as continuous parallel and curvilinear ridges at regional scale (Fig. 1A – white arrow) on the basis of Viking Orbiter data (Lockwood et al., 1992). However, the wealth and increasing resolution of remotely sensed imagery showed it is comprised of both randomly (Fig. 1A – black arrow) and highly organized (Fig. 1A – white arrow) spatial patterns of individual pitted cones/small mounds that lie above lobate deposits. Thumbprint terrain overlies millions of square kilometres primarily in the northern plains between 30°N and 50° (e.g., Acidalia Planitia, Utopia Planitia, etc...), although they also occur in a large area near the Martian equator (i.e., Isidis Planitia). Several hypotheses have been proposed for the origin of thumbprint terrain; with the majority of them involving the presence of ice/water. The individual cones were first interpreted as possible pseudo-craters formed by explosions associated with lava emplacement over wet ground (Frey and Jarosewich, 1982; Carr, 1986), cinder cones (Scott et al., 1995), pingos, ice-cored ridges (Lucchitta, 1981; Rossbacher and Judson, 1981), moraines (Lucchitta, 1981; Scott and Underwood, 1991; Kargel and Strom, 1992; Lockwood et al., 1992), or mounds formed by the disintegration of stagnant ice covers (Grizzaffi and Schultz, 1989). According to the most recent hypotheses, they are interpreted as mud

volcanism-driven deposits (Tanaka et al., 2003; Salvatore and Christensen, 2014), liquefaction deposits (Skinner et al., 2008; Skinner and Fergason, 2010) or related to impact-generated tsunami lobate deposits (Rodriguez et al, 2016; Costard et al, 2017; Costard et al., 2019).

On Earth, the most common triggers of tsunamis are earthquakes, subaqueous landslides, and volcanic activity. Only on rare occasions meteorite crashes give rise to tsunamis, thus terrestrial impact-induced tsunami deposits are sparse (Paris et al., 2009; Bryant, 2001). Conversely, on Mars, impact-generated tsunamis seem to be a plausible trigger mechanism. The study area (SE Acidalia Planitia) is uniquely positioned in that numerical modelling and geologic investigation tie an asteroid impact (e.g., Lomonosov crater) to the generation of a tsunami wave (Iijima et al., 2014; Rodriguez et al, 2016; Costard et al, 2017; Costard et al., 2019) that extended to the areas covered by thumbprint terrain. These numerical predictions, combined with geologic observations, demonstrate the importance of the study area and provides a convincing scenario for thumbprint terrain origin.

Here, we focused on thumbprint terrain (or TT), i.e. alignments of cones or mounds, in the southeastern Acidalia Planitia near the dichotomy (43°-53° N 0°-22° E; Fig. 1B), in an effort to: (i) characterize their geographical distribution; (ii) describe their morphology and relationship with former/underlying topography around the dichotomy and (iii) discuss their origin considering evidences and regional geological context. We will refer to alignments of cones/mounds simply as “thumbprint terrain” or “TT”; while we will refer to both thumbprint terrain and underlying associated lobate deposits as “lobate TT unit”. Although lobate deposits were not the focus of this study, it is useful to have a terminology that indicates both thumbprint terrain and underlying lobes when discussing the overall evolution of the area since target morphologies (TT) are closely related to lobate deposits in SE Acidalia Planitia.

2 Stratigraphy

The Vastitas Borealis Formation is the most widespread formation in the northern lowlands (Greeley and Guest, 1987; Tanaka and Scott, 1987). Many different hypotheses have been proposed to explain its origin, supporting either a sedimentary

processes related to outflow channels (Kreslavsky and Head, 2002) or a volcanic process (Catling et al., 2012). Kreslavsky and Head (2002) asserted that a sedimentary section of the Vastitas Borealis Formation formed as a residue when water from the outflow channels settled, quickly froze, and then sublimated. However, recent studies suggested that portions of Vastitas Borealis Formation were emplaced and/or modified while still saturated with liquid water (McGill and Hills, 1992; Tuckwell et al., 2003; Buczkowski and Cooke, 2004; Cooke et al., 2011; McGowan, 2011; Buczkowski et al., 2012). Regional geologic mapping (Tanaka et al., 2005; Fig. 2) separated the Vastitas Borealis Formation into two distinct units: the interior (ABvi) and the marginal unit (ABvm). The ABvi unit is the more extensive of the two units and hosts most of the diagnostic Vastitas Borealis Formation morphological features (Salvatore and Christensen, 2014). Data from Mars Orbiter Laser Altimeter (MOLA) derived Digital Elevation Model (DEM) and several 100-m/pixel-resolution Thermal Emission Imaging System images (THEMIS) reveals that the ABvi unit is rougher and has a higher thermal inertia than the ABvm unit (Tanaka et al., 2005, and references therein). The ABvi unit also consists of relatively bumpy, plains-forming material (Tanaka et al., 2005) that covers most of the northern plains including Vastitas Borealis and Utopia, Acidalia, and northern Arcadia Planitiae. The outer parts of the ABvi unit include the lobate TT unit (Fig. 2), as well as random clusters of hills mostly <1 km across (Frey and Jarosewich, 1982; Grizzaffi and Schultz, 1989; Scott et al., 1995). Approaching the edge of the unit, cones/mounds tend to decrease in quantity, occurring in random and small groups until their complete disappearance (Tanaka et al., 2005; Salvatore and Christensen, 2014). Conversely, the ABvm unit outcrops surround the ABvi in Utopia Planitia, along Arabia Terra, in southern Acidalia Planitia, north of Alba Patera, and in western Arcadia Planitia. At lower latitudes (< 25° N), it appears smoother, exhibits a higher albedo and lower thermal inertia than both the ABvi unit and surrounding materials in THEMIS daytime infrared images. This means that the ABvm unit is warmer, which may indicate a relatively fine-grained material compared to adjacent materials (Tanaka et al., 2005). Parts of the ABvm are buried by Amazonis and Elysium provinces materials. The ABvm unit also includes systems of fretted valleys that are a few kilometres wide and tens of kilometres long (Squyres, 1978; Carr, 1995; Tanaka et al., 2005). These features have no clear terrestrial analogues and they have previously been compared to glacial moraines and kame complexes (Lucchitta, 1981), glacial tunnel valley and esker features (Kargel et al., 1995), or soft-sediment deformation structures (Tanaka et al.,

2003). The Vastitas Borealis marginal and interior units generally have a poorly defined contact and post-emplacment material evolution. In addition, the southern limit of the collective outer margin of both Vastitas Borealis units is fairly constant in elevation ($\sim 3900\text{m} \pm 70\text{m}$) and close to the mean elevation of the Deuteronilus contact (see section 1), hence it may indicate the presence of an ancient standing body of water (Parker et al., 1989, 1993; Head et al., 1999; Clifford and Parker, 2001; Carr and Head, 2003). In our study area, the Vastitas Borealis Formation approaches the Noachis Terra unit (Nn) (Fig. 2) and to a lesser extent the Deuteronilus Mensae 1 unit (HBd1; Mangold et al., 2002) (Fig. 2). The Noachis Terra unit is Middle to Late Noachian in age and represents mostly heavily cratered terrain (Tanaka et al., 2005). Most of the unit displays layering (Malin and Edgett, 2001), in MOC narrow-angle data. Elevation ranges between $-2,000$ and $-5,000$ m within the northern plains across Orcus Patera and Acidalia Mensa (Tanaka et al., 2005).

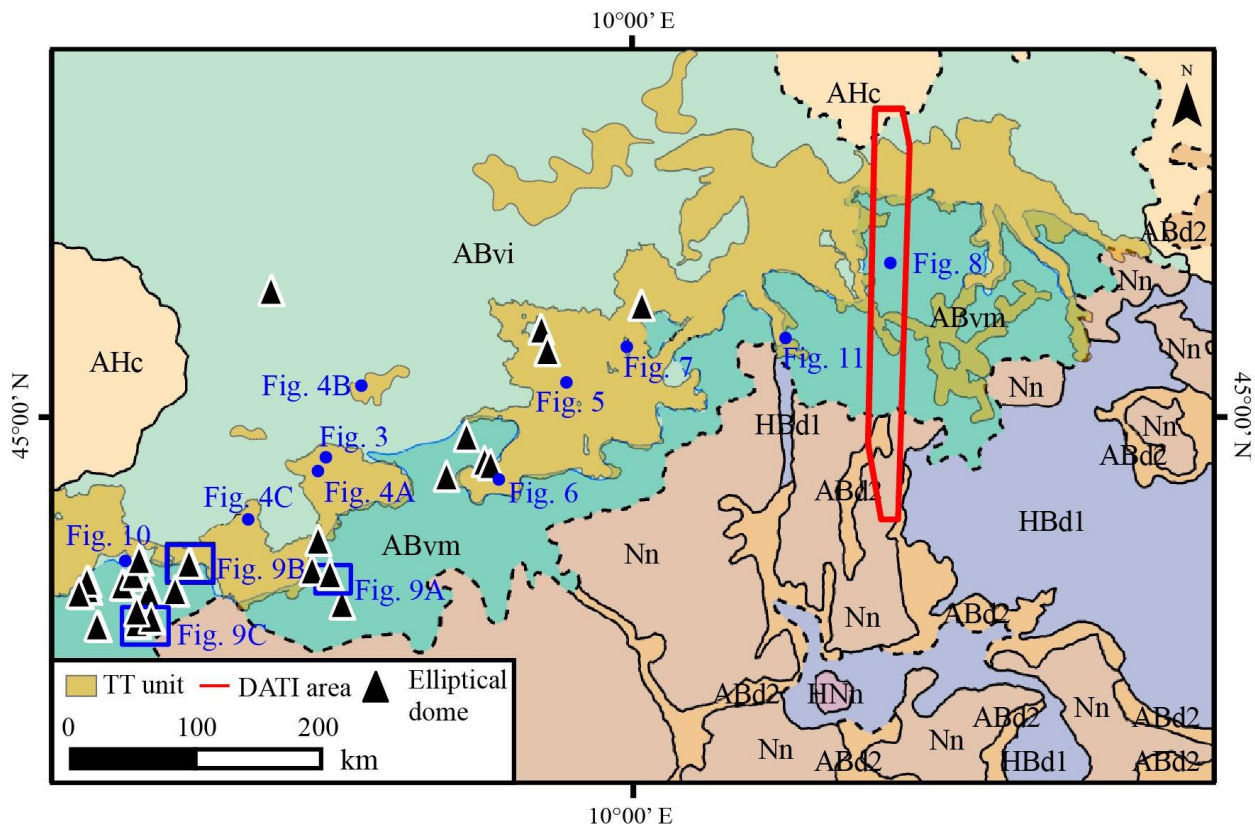


Figure 2. Background geological map is 'US Geological Survey Sci. Inv. Map 2888' by Tanaka et al., 2005. Lobate TT unit extension is marked by the orange polygons and covers an area bigger than 10^5 km². Red frame indicates the area of quantitative thermal inertia analysis (See section 3). Elliptical domes related to the thumbprint terrain (see Fig. 9-10) are localized outside or along the boundary of the thumbprint area (black triangles are not to scale). The lobate TT unit was mapped crossing both the Vastitas Borealis interior unit (ABvi) and Vastitas Borealis marginal unit (ABvm). Other geologic units: Nn - Noachis Terra Unit; HBd1 - Deuteronilus Mensae unit 1; ABd2 - Deuteronilus Mensae 2 units; HNn -

Nepenthes Mensae unit. See Tanaka et al. 2005, for a more complete description. Courtesy of NASA/USGS.

3 Data and Methods

Context Camera (CTX; 6m/pixel) (Malin et al., 2007) and High Resolution Imaging Science Experiment (HiRISE; 0.25-0.32m/pixel) (McEwen et al., 2007) images were used to investigate thumbprint terrain. CTX images provided a full coverage of the study area to be compared with Mars Orbiter Laser Altimeter (MOLA; Smith et al., 2001) digital elevation model (DEM) which provided the topographic base map with a spatial resolution of 463 m. Detailed topographic profiles were performed from MOLA laser shots (vertical resolution: 50 cm; size of the laser shot on the surface: 128 m) to investigate and to provide a topographic context for TT morphologies and associated lobate deposits (e.g. Fig.3 and following) thanks to MOLA Precision Experiment Data record (PEDR) facility available at the Photothèque Planétaire d'Orsay, France (<http://fototek.geol.upsud.fr/-Mars-Orbiter-Laser-Altimeter-.html>). Mars Odyssey (ODY) Thermal Emission Imaging System (THEMIS) daytime and night-time infrared (IR) images (100m/pixel; Christensen et al., 2004) were also used to investigate the thermo-physical properties, including thermal inertia that quantifies the physical properties and average particle sizes of surface textures and morphologies (Ferguson et al., 2006). Relief characteristics (slopes and aspects) for the relief correction of albedo and temperature difference (input parameters in Eq. 1) were calculated based on the High Resolution Stereoscopic Camera (HRSC) DEM-s (spatial resolution: 100 m; Neukum and Jaumann, 2004; Jaumann et al., 2007) in *da4.img format (aeroid directly comparable with MOLA grid) acquired from Mars Orbital Data Explorer (<http://ode.rsl.wustl.edu/mars/>).

3.1 Thermal inertia estimation

We performed a quantitative detailed analysis of thermal inertia on a selected portion of the studied area (Fig. 2). As direct measurement of thermal inertia was not possible to estimate; Differential Apparent Thermal Inertia (DATI) was computed as follows:

$$DATI = \frac{1-A}{\Delta T} \quad [\text{Eq. 1}]$$

- 1 where A is the albedo and ΔT is the temperature difference. DATI technique (Sabol et
- 2 al., 2006) is proportional to P ('direct' thermal inertia) and is calculated based on short

3 time (t) intervals (at least one hour time difference) with a high $|\Delta T/\Delta t|$ gradient (in the
4 morning or in the afternoon), preferably during the same period of the year (similar solar
5 longitude). The selected part of SE Acidalia Planitia was chosen on the base of: (i) data
6 availability for DATI calculation (i.e., high quality images with appropriate time interval,
7 in the same period of the year), and (ii) the presence of the key landforms (thumbprint
8 terrain). THEMIS IR images were processed online using the Themis Processing Web
9 Interface (THMPROC; <http://thmproc.mars.asu.edu>). To calculate the Differential
10 Apparent Thermal Inertia (Eq. 1), high quality THEMIS images were chosen: the
11 minimum and maximum “summing” parameters were set to 1 (full-resolution images),
12 while the minimum and maximum “image rating values” were set to 4 and 7,
13 respectively. These parameters depend on a subjective assessment of the image
14 quality ranging from 1 (unusable) to 7 (very good); this assessment includes
15 consideration of exposure, missing lines, instrument noise, and atmospheric features.
16 Relief correction for A and ΔT was also performed since this kind of calibration is not
17 included in thermal inertia modelling. Temperature difference (ΔT) was additionally
18 calibrated against total incoming energy. Atmospheric correction was also included. In
19 order to avoid large errors by calculating DATI and albedo, the cells with $i > 79^\circ$ were
20 excluded from the calculations.

21 The uncertainty in DATI calculation arises from errors due to dust opacity, albedo and
22 slope inclination. The errors in daytime THEMIS temperatures may be ± 3 K (Ferguson
23 et al., 2006). Assuming the temperature amplitude is 20 K and albedo is 0.2, a ± 3 K
24 error implies 17% relative error on thermal inertia due to the error of each of two
25 measured temperatures. Dust opacity is $1.6 \text{ J m}^{-2} \text{ K}^{-1} \text{ s}^{-1/2}$ making up 0.8% of the
26 average DATI, ($200 \text{ J m}^{-2} \text{ K}^{-1} \text{ s}^{-1/2}$), and standard deviation (SD) due to seasonal
27 variation of dust opacity in the high-dust season, which is 0.1. We estimate that a dust
28 opacity error of 0.1 generates a relative error of 5.6% on apparent thermal inertia by
29 comparing average DATI values corrected for dust opacities of 0.22 (average), 0.32
30 (average +1 SD) and 0.12 (average -1 SD). Considering the two errors of 0.8% and
31 5.6%, the total uncertainty related to dust opacity is 5.7% when applying the rule of
32 error propagation for error addition. The uncertainty of albedo calculation is 8% which
33 generates a 1.5% error on DATI values. The error in computation of slope inclination on
34 HRSC DTM is $\sim 4^\circ$ (Heipke et al., 2007), which can potentially add up to 35% of error on
35 DATI values where the incidence angle is very high (79°). This is calculated by

36 comparing DATIs for 79° to the average DATI for 75° and 83°, provided all other
37 parameters are fixed at typical values. In the most common case where the incidence
38 angle is in the range 0°– 50°, the DATI error is within 10%. Taking temperature, dust
39 opacity, slope inclination and albedo into account, the total uncertainty on DATI is
40 estimated to be within 27%. However, it can reach up to 43% when the incidence angle
41 is 79°.

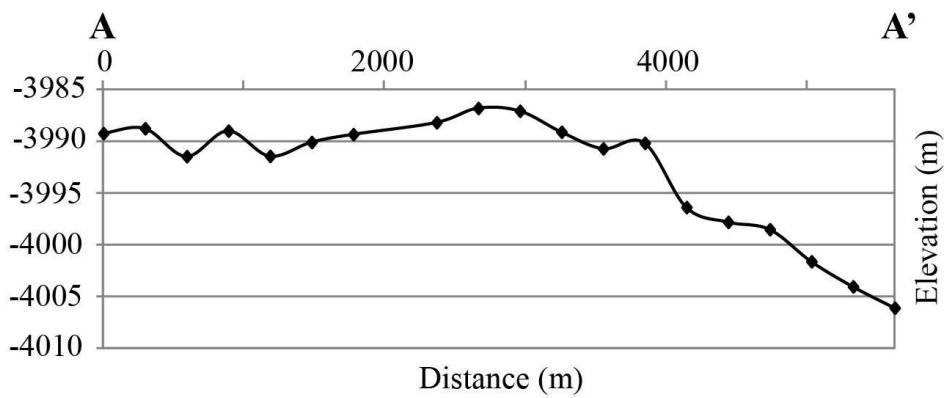
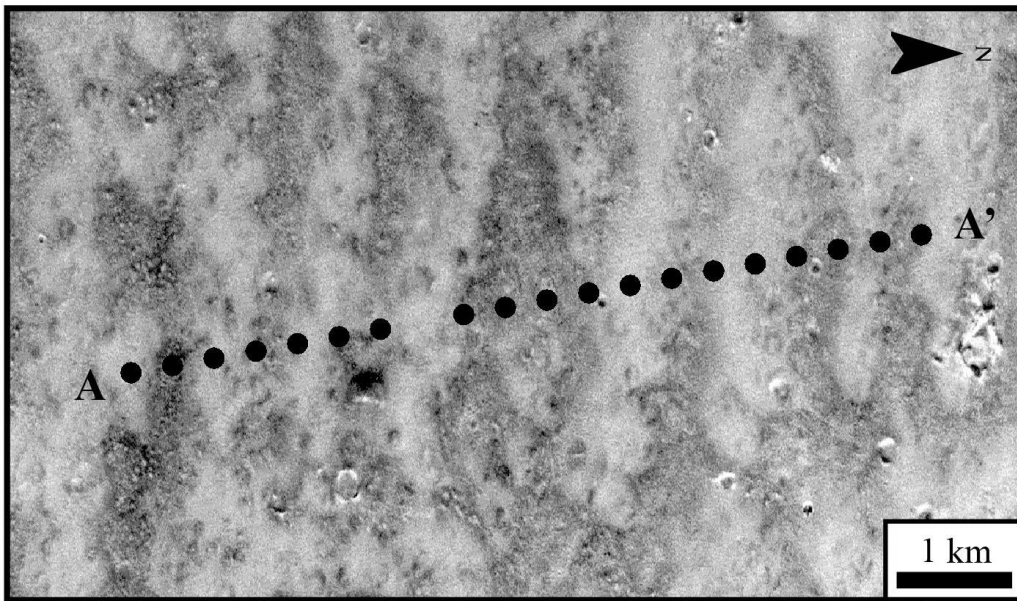
42

43 **3.2 Crater-size frequency distribution**

44 We performed a crater counting analysis using CTX imagery to provide an age
45 estimation for the lobate TT unit deposits. All visible impact craters (>500 m in diameter)
46 were measured except the aligned secondary clusters and rays within the CTX
47 resolution limit using the ArcGIS add-in CraterTools (Kneissl et al., 2011; Bamberg et
48 al., 2013). The crater-size frequency distribution (CSFD) was plotted and the crater
49 retention ages were calculated with Craterstats by visually selecting the portion of the
50 crater size-frequency distributions that is parallel to some isochrons between steps of
51 the distribution (Neukum, 1983; Hartmann and Neukum, 2001; Platz et al., 2013).

52 **4 Results**

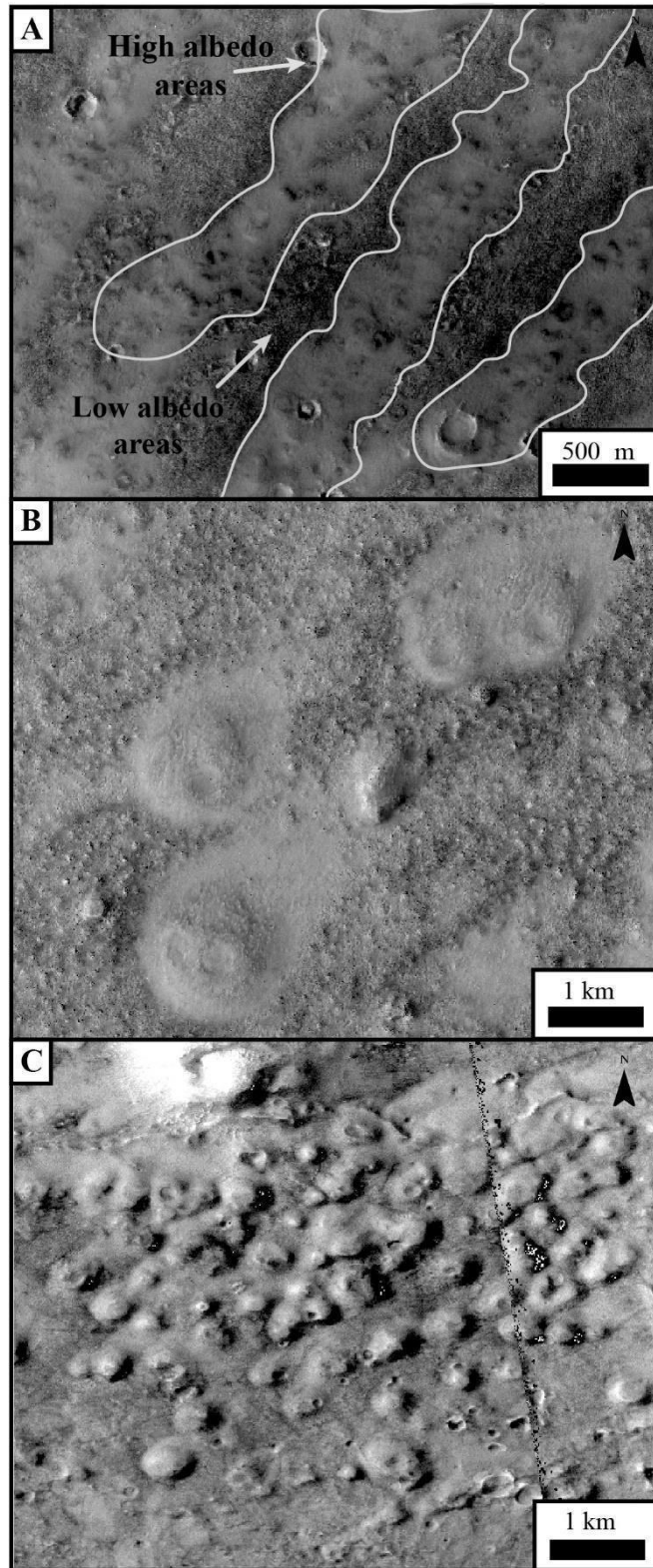
53 Thumbprint terrain was usually described as sets of alternating ridges/mounds and
54 depressions, with high and low albedo respectively, up to several tens of kilometres in
55 length (Fig. 1A; Lockwood et al., 1992). However, we observed no noticeable variations
56 of alternating relief by using MOLA laser shots in our study area (Fig. 3). The low albedo
57 surfaces show a darker rough surface, while the high albedo areas show alignments of
58 poorly expressed mounds (Fig. 4A) that can individually be dome-like (Fig. 4B) or more
59 rarely conical (Fig.4C) when seen at high resolution.



61

62

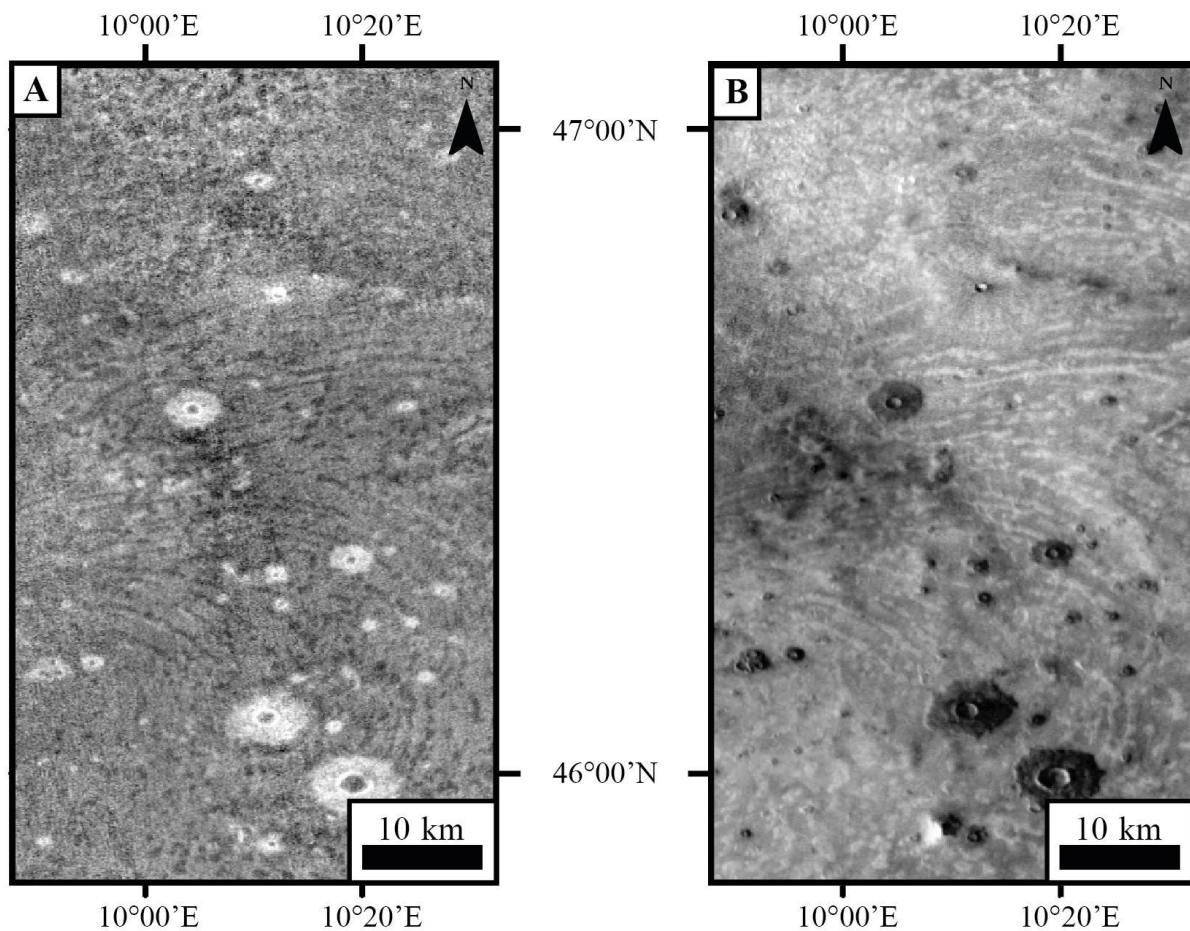
63 *Figure 3. Topography of the thumbprint terrain. A topographic profile crossing the high and low albedo*
 64 *area was performed by using MOLA laser shots. No clear topographic alternation is observed between*
 65 *the two areas. The black points represent the approximate size of the laser shot on the surface (128m)*
 66 *according to Smith et al., 1999; 2001 (CTX image n° B17_016195_2250). North is oriented 90 degrees*
 67 *right. Courtesy of NASA/ JPL/Univ. of Arizona.*



68

69 *Figure 4. Morphology of thumbprint terrain at high resolution. A) High albedo areas include mounds and*
 70 *pits while low albedo areas are composed of a rough surface (HiRISE image: ESP_011949_2255). The*
 71 *high albedo areas of the thumbprint terrain include mounds that may be B) dome-like (HiRISE image:*
 72 *PSP_001928_2265) or more C) cone-like shaped mounds (CTX image: P22_009747_2239). The former*
 73 *type is usually bigger in diameter than the latter, but no clear correlation was found. Courtesy of JPL/Univ.*
 74 *of Arizona.*

75 Thermal inertia comparisons showed that thumbprint terrain is brighter than the
 76 surrounding terrain in day-time THEMIS images, whereas it is darker in night-time ones
 77 (Fig. 5). Moreover, the whole lobate TT unit is also generally brighter in day-IR images
 78 in comparison to the surrounding plains and plateau units, so we readily defined the
 79 lobate TT unit limit realizing: (i) TT is also present in the ABvm unit, although previous
 80 literature (Tanaka et al., 2005) considers that it extends only within the ABvi unit (Fig. 2)
 81 and (ii) it covers an extensive surface greater than 10^5 km² in southeastern Acidalia
 82 Planitia.

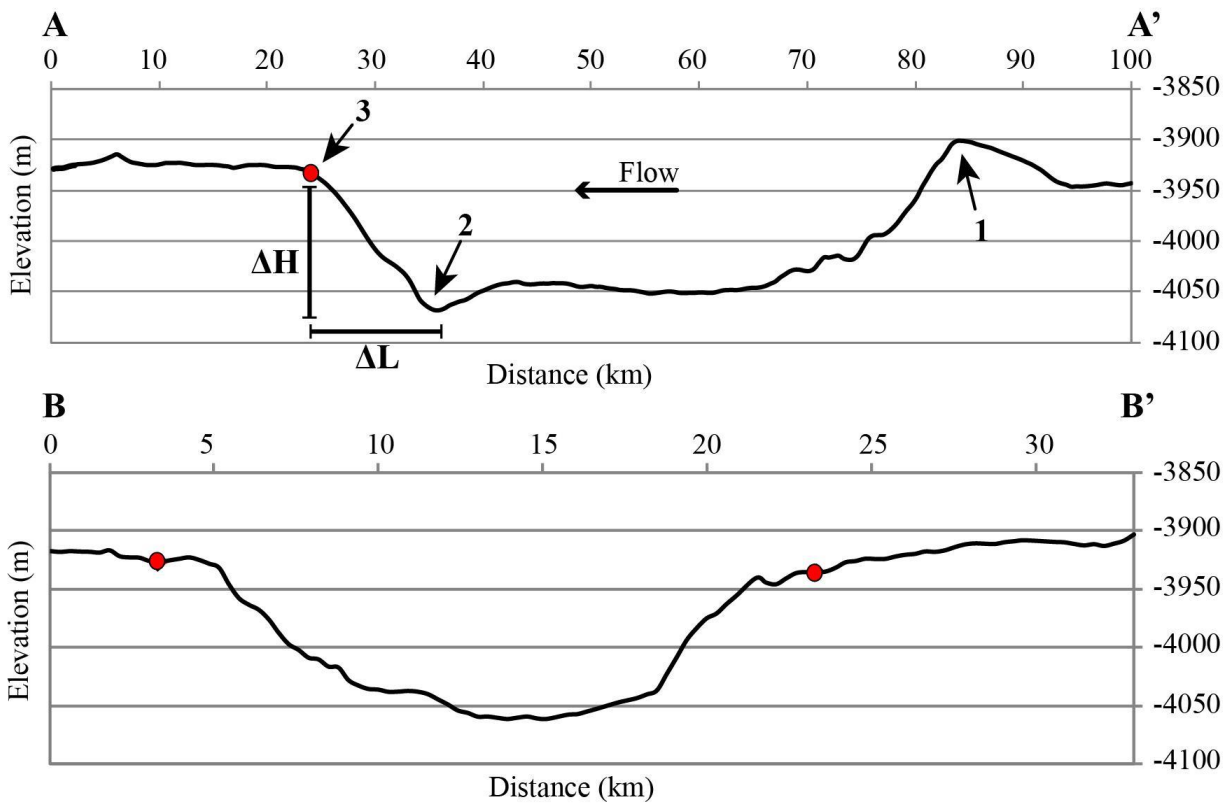
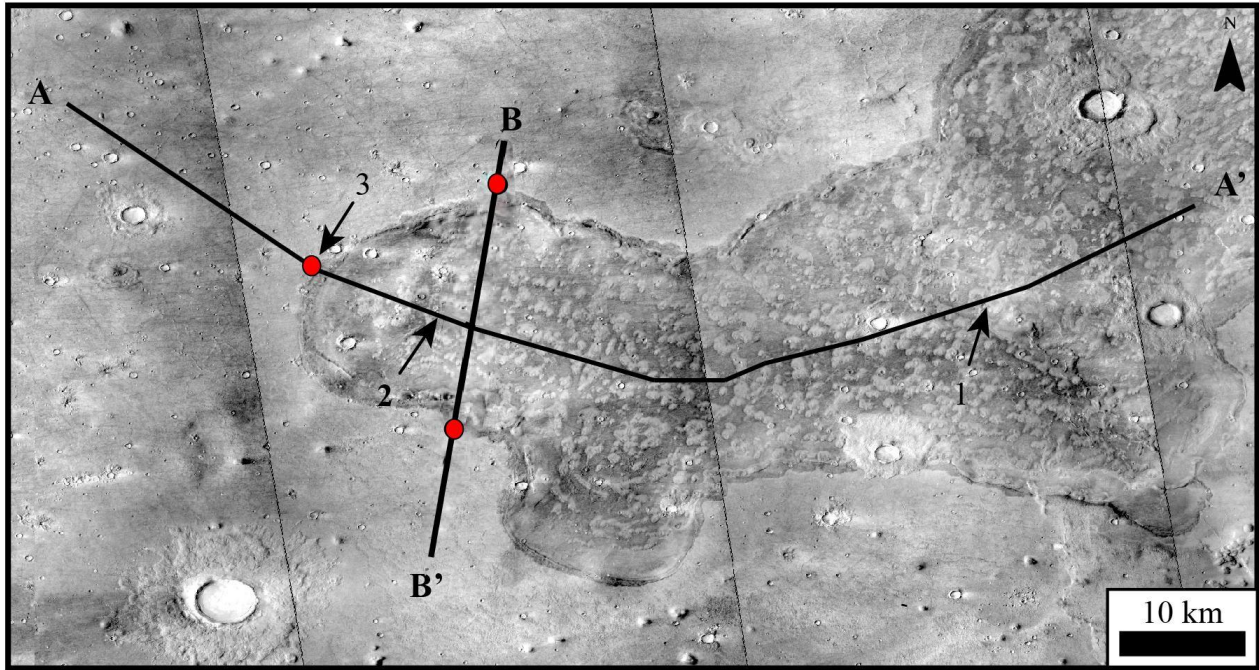


83
 84 *Figure 5. THEMIS daytime and night-time infrared images of thumbprint terrain. The low albedo areas are*
 85 *darker in night-time images (A) and brighter in daytime ones (B). Night-time image resolution is lower than*
 86 *the daytime resolution.*

87 Unfortunately, the northern limit of the lobate TT unit in Acidalia Planitia is covered by a
 88 unit of lower albedo that has a constant elevation of around -4100m (supplementary
 89 material). Therefore, the true extent of the unit remains unknown. In the southern region
 90 of the study area, the lobate TT unit covers the plateau and valleys near the dichotomy.
 91 The southern boundary of the unit is marked by several lobate features with peripheral
 92 and lateral ridges that sometimes overlap each other in the Deuteronilus valley system

93 (Costard et al., 2017). The lobes are found inside valleys or on lateral valley plains
94 between -3860 m and -4001 m altitude.

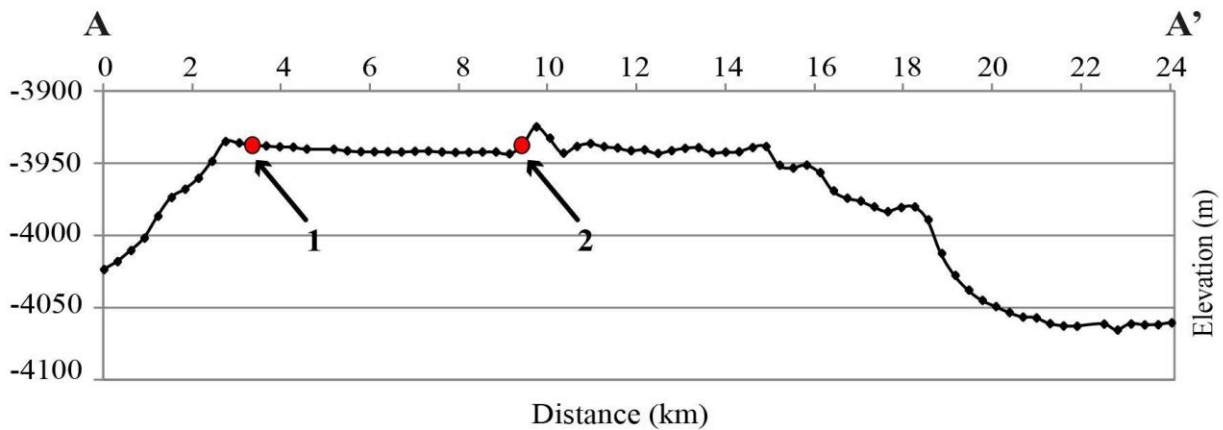
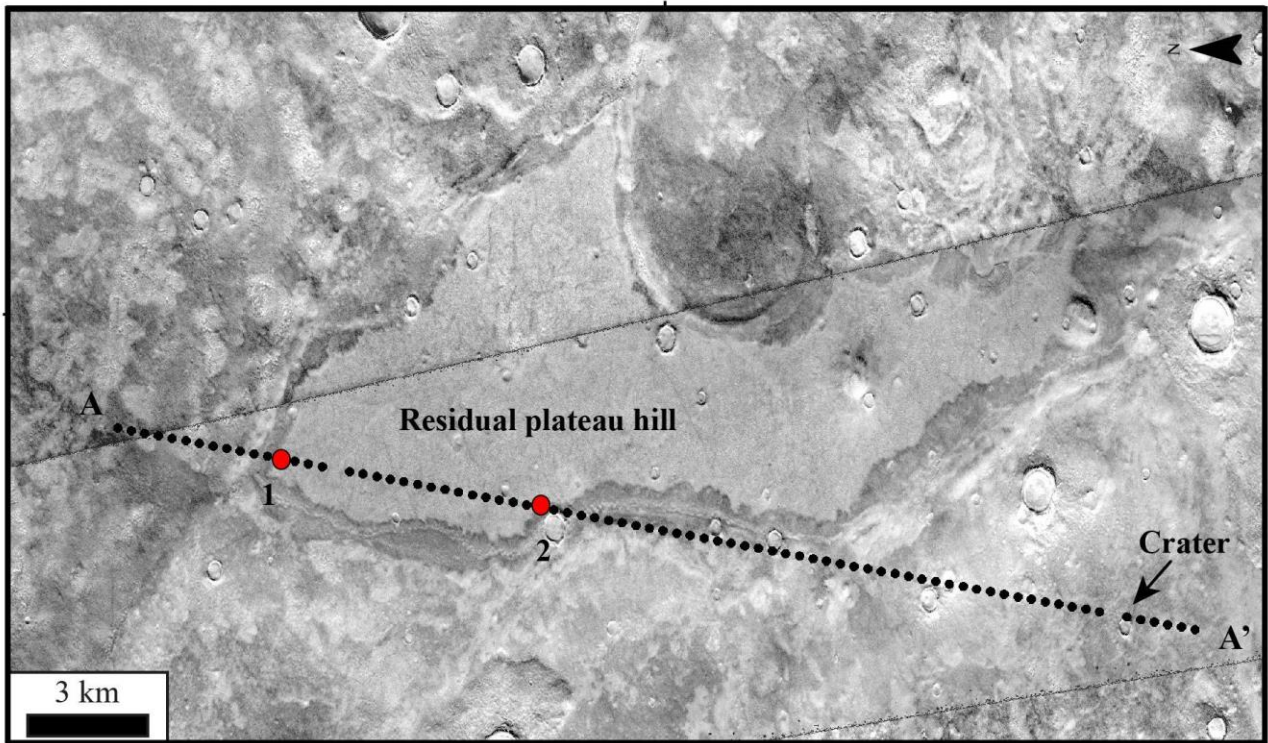
95 We also observed that lobes are oriented upslope of few degrees (Fig. 6), or on residual
96 hills plains (Fig. 7), reaching a maximum thickness of 10-20 m by using MOLA laser
97 shots (Costard et al., 2017). Occasionally, the characteristic alignments of
98 cones/mounds tend to distance themselves approaching the edge of the lobate TT unit
99 and do not show the characteristic high albedo small mound chains. Regardless, we
100 included them in the thumbprint terrain unit due to thermal inertia comparisons with
101 surrounding areas, lateral continuity and sparse presence of clusters or individual small
102 mounds. A general southeastward trend has been computed from the analysis of the
103 high albedo mounds (Fig. S1 - supplementary material), even if there are some lobes
104 with random direction because of first-order topographic influence (Fig. S2 -
105 supplementary material).



106

107

108 *Figure 6. Longitudinal profile (A-A') and cross-section (B-B') of a southern limit lobate TT unit deposit from*
 109 *MOLA DEM. $\Delta L=12000m$; $\Delta H=138m$. Lobate TT unit limits are marked by red dots on the image and on*
 110 *profiles as well. Relative slope value is $\approx 0.70^\circ$. CTX images: P18_008112_2251; P18_007901_2250;*
 111 *P18_008046_2253; P21_009338_2253.*

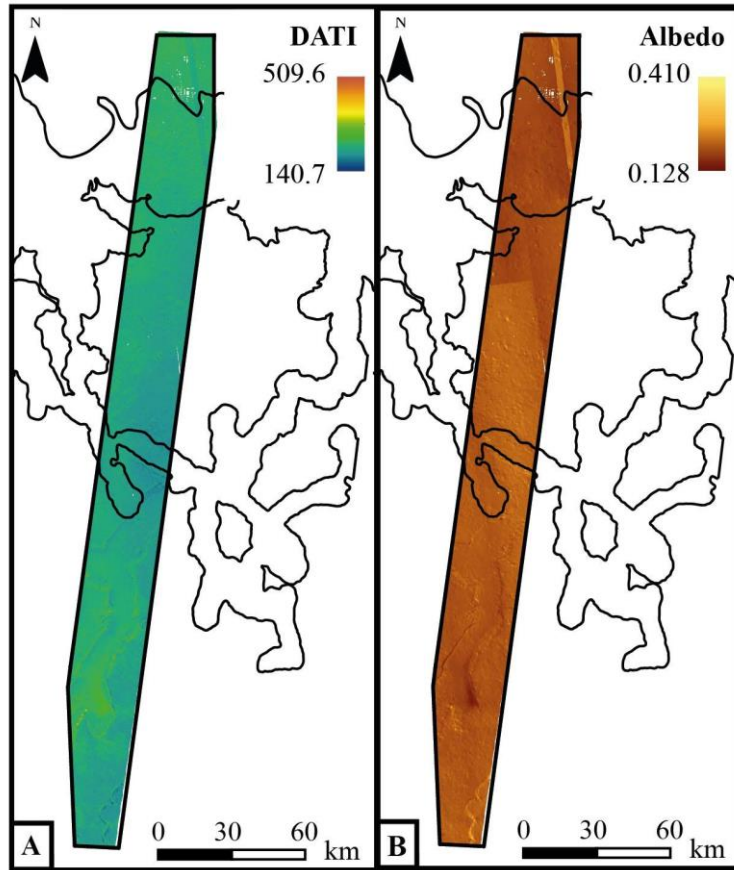


112

113 *Figure 7. Thumbprint terrain deposits can move upslope reaching plateau residual hills. Thumbprint*
 114 *terrain limit that is marked by red dots on the image and on A-A' MOLA shots profile as well (CTX image:*
 115 *B02_010261_2248). North is oriented 90 degrees left.*

116 Thermal inertia was calculated based on the IR THEMIS data for the part of the
 117 thumbprint terrain unit (marked by the black line on Fig. 8A). For this area, DATI values
 118 ranges from 171 to 311 indicating fine particles (~40 – 500 μm : silt to medium sand)
 119 with the average particle size of 125 μm (Ferguson et al., 2006; Wentworth, 1922). An
 120 average albedo of 0.19 (range 0.15-0.33) calculated for this region based on CTX
 121 images further supports the presence of silt and fine sand. (Fig. 8 B).

122



123

124 Figure 8. Thermal inertia analysis. A) DATI ($J m^{-2} K^{-1} s^{-1/2}$) values for the selected part of the study area
 125 shown in Fig.2. B) albedo values. Lobate thumbprint terrain unit extension is marked by the black line.
 126 The location of Fig. 8 is also shown in Fig.2. Top-left corner coordinates: $15^{\circ}39'58.366''E$;
 127 $49^{\circ}41'20.171''N$.

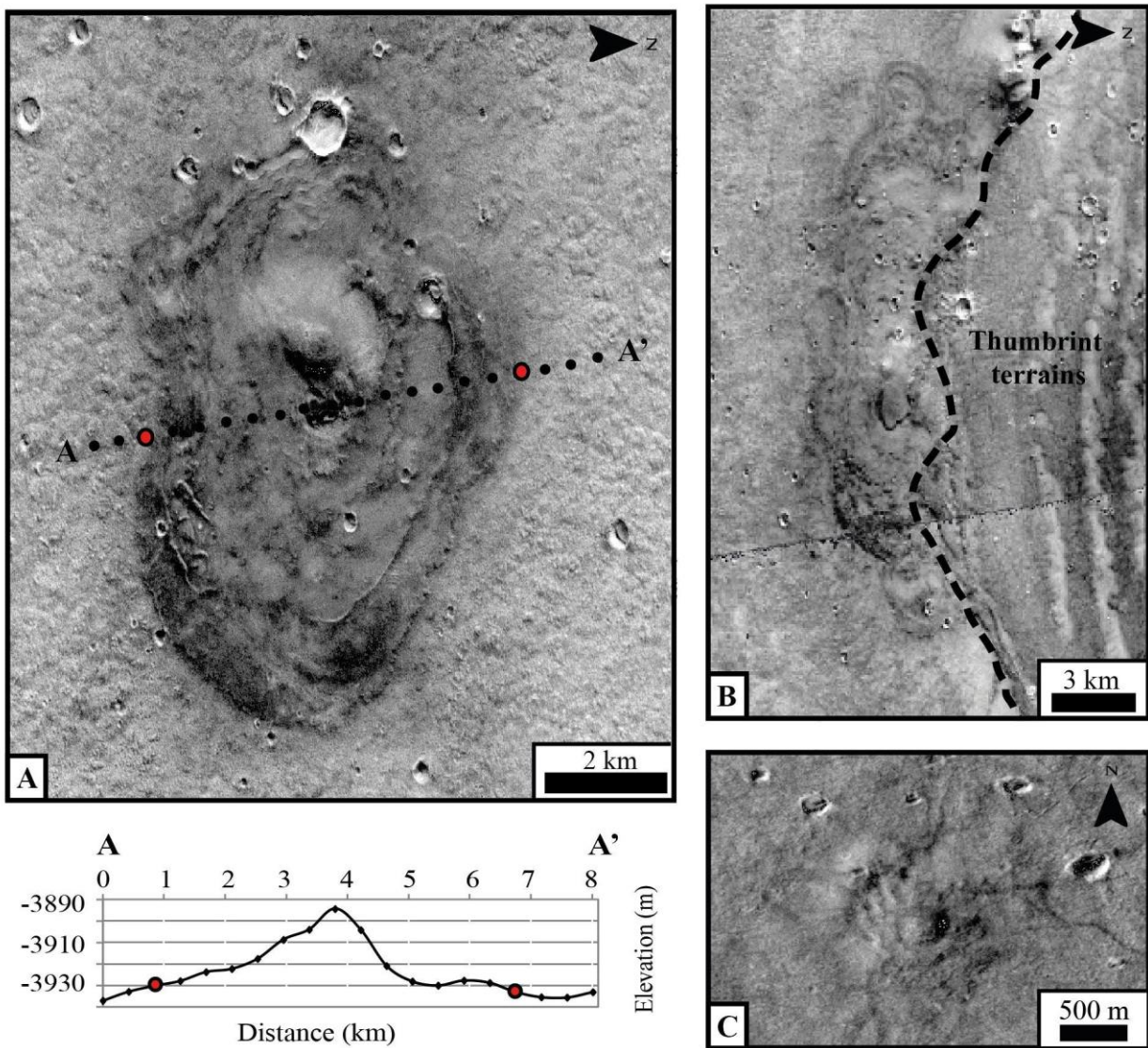
Material	DATI ($J m^{-2} K^{-1} s^{-1/2}$)	Particle diameters (μm)
Dust	~ 150	~ 45 (silt)
Sand	~ 200	~ 160 (very fine sand/fine sand)
	230-270	290 - 575 (medium sand)
Rock	1200	

128

129 Table 1. Comparative DATI values ($J m^{-2} K^{-1} s^{-1/2}$) and particles diameters (μm) of selected materials
 130 (after Ferguson et al., 2006).

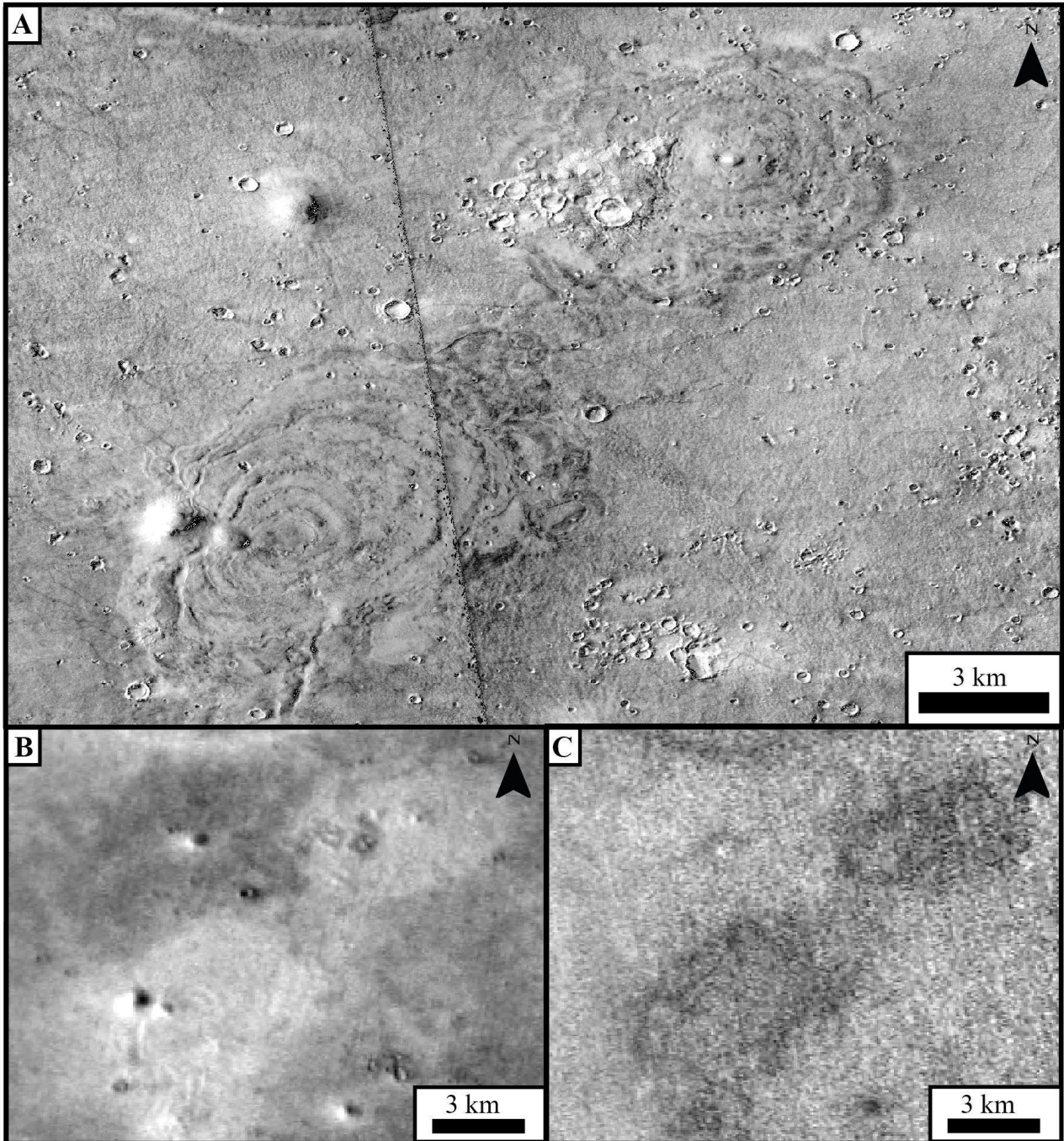
131 We observed several domes (10-12 kilometres in diameter) near or along the lobate TT
 132 unit limit (Fig. 2), making their detection difficult inside thumbprint as the lobate TT unit
 133 overlaps them (Fig. 9B). These morphologies are mostly elliptical, have an irregular and
 134 lobate edge and show concentric features compared to the central peak (Fig. 9A; Fig.
 135 9B). Smaller features (≈ 1 km in diameter) are observed, but are almost circular and do

136 not show clear concentric lineaments (Fig. 9C). MOLA elevation profiles showed they
 137 have a symmetric profile and heights of few tens of meters as shown in Fig. 9A.
 138 Thermal inertia comparisons show that these domes are very bright in day-IR images
 139 and darker in the night compared to the surrounding units (Fig. 10). This characteristic
 140 is qualitatively similar to the response that thumbprint terrain has to night/day material
 141 exposition. In fact, TT is also generally brighter in day-IR images, whereas it is darker
 142 during night acquisition (Fig. 5).



143
 144 *Figure 9. Large domes underlying thumbprint terrain unit. A) MOLA laser shot cross-section cutting a*
 145 *dome that is found outside thumbprint terrain unit. Central peak and some relating concentric*
 146 *features are visible. The edge is elliptical and quite regular. The boundary is marked by red dots.*
 147 *Dome height is $\approx 40\text{m}$ (CTX image: B17_016195_2250). North is oriented 90 degrees right. B) Dome*
 148 *overlapped by thumbprint terrain. Black dashed line marks thumbprint terrain unit limit. Central peak,*
 149 *some concentric features and an irregular and lobate edge are observed. (CTX image:*

150 P21_009391_2238). North is oriented 90 degrees right. C) Small circular dome that does not show a
151 clear/regular limit or concentric features related to the centre (CTX image: G23_027087_2234).



152

153

154 *Figure 10. Large domes several kilometres across underlying thumbprint terrain unit in visible CTX-scale*
155 *(A). Thermal inertia response in day- and night-time acquisitions. THEMIS images show that domes are*
156 *brighter in daytime (B) and darker in night-time (C) compared to surrounding areas. Night-time image*
157 *resolution is lower than daytime image. CTX images: P21_009246_2240; G23_027087_2234.*

158

159 5 Discussion

160 Since the most recent hypotheses have already provided a regional geological
161 framework for lobate deposits in Acidalia Planitia (Rodriguez et al, 2016; Costard et al,
162 2017; Costard et al., 2019), in the following paragraphs we will discuss and consider
163 the characteristics of thumbprint terrain to each of the main geological scenarios (i.e.,
164 pingoes, volcanic cones, liquefaction, mud-volcanoes, and tsunami-related deposits) in
165 order to reconcile and insert TT origin in the regional context.

166 Although the scenario of a periglacial environment has been put aside in favour of more
167 conceivable interpretations in the last years, Rodriguez et al. (2016) did not totally
168 dismiss this hypothesis because tsunami deposits could have frozen and formed a layer
169 of permafrost. Moreover, the presence of excess ejecta craters strengthens the
170 occurrence of an icy sub-surface layer that could also be responsible for surficial
171 geological processes as proposed for other geological processes in other areas on
172 Mars (Salese et al., 2016). However, pingoes are domical structures formed by freezing
173 and swelling of groundwater and are, therefore, composed by the same material as their
174 surroundings. Thus, the difference observed between the pitted mounds and the darker
175 adjacent areas in THEMIS images are not consistent with a pingo hypothesis (Fig. 5).
176 Furthermore, the growth of pingoes is accompanied by radial extension cracks (Mackay,
177 1973; 1998), which were not observed in any of our target features and deposits. The
178 high albedo mounds have been also interpreted as moraines, or ice-cored ridges
179 associated with a former glacial environment (Lucchitta, 1981; Rossbacher and Judson,
180 1981; Farrand and Gaddis, 2003), but their exact origin is still under debate. Herein, we
181 find the periglacial origin hypothesis problematic because of thermal inertia
182 comparisons with surrounding deposits (Fig. 5), material viscous behaviour that is not
183 consistent within a periglacial or glacial environment, and the lack of typical glacial
184 features such as polygons, cracks, eskers, drumlins and kettle holes.

185 Alternatively, over many decades, the associated underlying TT lobate deposits have
186 also been interpreted as lava flows flooded over a broad region forming a volcanic plain.
187 In this scenario, the high albedo mounds are interpreted in a variety of ways including:
188 1) rootless cones (pseudocraters) formed by explosions that resulted from a lava flow
189 advancing over a wet substrate (Frey and Jarosewich, 1982); 2) cinder cones formed by
190 explosion and deposition of ashes (Wood, 1979); or 3) tuff cones resulting from the
191 explosive interaction between rising magma and water/groundwater (Wohletz and
192 Sheridan, 1983). However, thumbprint terrain mounds are brighter than basaltic sands

193 in Acidalia (Farrand et al., 2005) and the DATI values of the TT are much lower than the
194 ones expected for lava flows (Fig. 8; Table 1). In addition, volcanic cones do not form in
195 arrangements that resemble patterns observed within TT. Based on the lack of these
196 conditions, we conclude that a volcanic origin of the thumbprint terrain is unlikely for TT
197 in southeastern Acidalia Planitia.

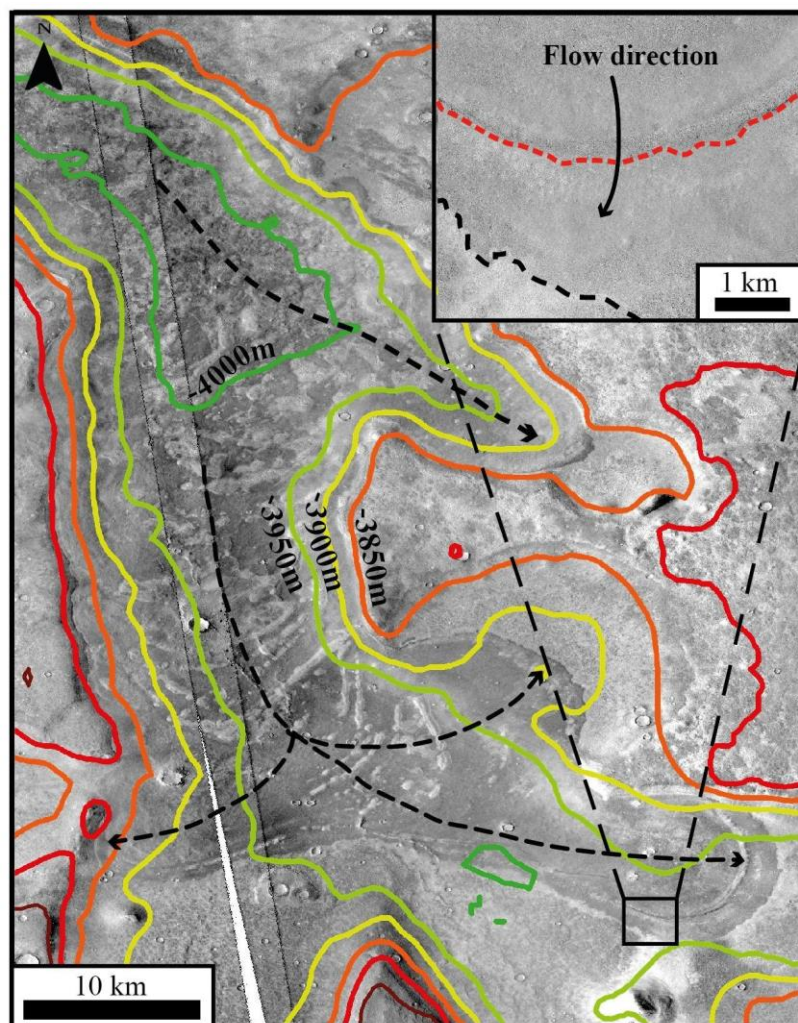
198 More recently, thumbprint terrain has also been interpreted as mud volcanoes which
199 formed after the freezing of an ancient standing body and/or rapid sedimentation and
200 diagenesis. The existence of a mud sheet flood has also been proposed for the northern
201 lowlands due to some hills and ground undulations in Isidis Planitia and Mare Australe
202 (Farrand et al., 2005; Oehler and Allen, 2010; Souček et al., 2015; Komatsu et al.,
203 2016). As outflow channels filled northern lowlands (Baker et al., 1991; Carr and Head,
204 2003), the following ice sublimation mostly depended on the accumulation rate of debris
205 on the surface. Sublimation residue would have formed the Vastitas Borealis Formation
206 units. Even a shallow layer of little debris thickness would have decreased sublimation
207 and favoured freezing (Farmer and Doms, 1979; Carr, 1990; Carr and Head, 2003):
208 both the gradual freezing and the load of the top debris layer make the internal pressure
209 rise. This could have led to mixtures of water, ice, rock/soil and mud expulsion on the
210 surface as proposed in Utopia Planitia in order to explain etched flows and polygonal
211 troughs (Ivanov et al., 2014). This model can also be applied to the thumbprint terrain in
212 Acidalia Planitia since geologic observations and settings are similar. The high albedo
213 mounds could be analogous to terrestrial mud volcanoes with a wide range of different
214 features from meter sized cones to domical structures hundreds of meters in size
215 (Kholodov, 2002) that are similar in lateral and vertical dimension to the Martian domes
216 and cones of the Acidalia region. However, thermal inertia and albedo values indicate a
217 widespread presence of fine sand and silt (mud?) size grains. The reason could be
218 explained by two fundamental factors that eventually interacted with each other. First,
219 detectable grain-size values might not match mud particle size anymore since the
220 material dried up and got indurated over the time. Ultimately, sandy mud volcanoes
221 have been found on Earth (Miyakawa et al., 2013) and, thus, this phenomenon cannot
222 be excluded either.

223 Furthermore, we need to take into account the coexistence of TT with lobate underlying
224 deposits which points to flows with a certain viscosity: the lobate deposits with
225 peripheral ridges clearly indicate that viscous material flowed inside southern valleys

226 (Fig. 6; Fig. 11; supplementary material) and that the plateau and hills were partially
227 flooded (Fig. 7; Fig. S1- supplementary files). Additionally, parallel and arcuate
228 alignments of mounds/cones (thumbprint terrain) observed together around obstacles
229 as knobs, residual hills, and plateaus (Fig. 1A, white arrow, Fig. S1- supplementary
230 files), perfectly follow the inferred underlying lobate deposits flow direction (Fig. 11, Fig.
231 S1 and Fig. S2- supplementary material). In the occurrence of an impact-generated
232 tsunami: obstacles might have first influenced flow direction and speed (tsunami wave
233 fronts), forming thumbprint terrain in parallel and curvilinear patterns. Nevertheless, an
234 impact-generated tsunami provides an explanation to the main concern about the
235 energy required to flow up slopes and reach topographic heights. In a previous work,
236 three craters (30-50 km in diameter) were proposed (Fig. S3 - supplementary files) as
237 the sources of the tsunami events, based on validated terrestrial models scaled to Mars
238 (wave height, propagation, run up elevation, and distance) (Costard et al., 2017). The
239 numerical tsunami simulations presented in Costard et al. (2017) link the TT alignments
240 to interference patterns produced from the interaction between the tsunami fronts and
241 the coastal topography. By binding the numeric simulation results to the morphological
242 observations, we assert that a tsunami event contributed to the formation of TT mud-
243 volcanoes.

244 On Earth, tsunamis move landward in a series of wave fronts (Lavigne et al., 2009),
245 whose energy and interaction with the shoreline topography results in different
246 inundation distances and distributions of lobate debris. Within the complex topography
247 of flat-floored valleys and plateaus along the Martian dichotomy boundary, the
248 interference of the multiple reflected and refracted waves that are observed in
249 simulations explain the flow distribution itself and the origin of the arcuate and parallel
250 pattern that characterizes the thumbprint terrain. Thumbprint terrain cones are not
251 observed in any terrestrial tsunami, but they are herein considered mud volcanoes that
252 formed as a consequence to an overpressure caused by rapid compaction upon
253 deposition of the transported material during the final stage of a tsunami. A similar
254 geological process was proposed for the emplacement of the Vastitas Borealis
255 Formation in both Chryse and Acidalia Planitia at the regional scale (Salvatore and
256 Christensen, 2014). According to this hypothesis, the Vastitas Borealis Formation would
257 be a product of extensive sedimentary modification both during and immediately after
258 outflow channel activity. Mud-extrusion would then result from burial and rapid

259 compaction of previously saturated deposits (Salvatore and Christensen, 2014). In our
 260 study area, rapid compaction could have expelled a mixed water-mud material,
 261 preferentially along the front, and would explain 1) the arcuate or random pattern of
 262 thumbprint terrain reflecting the tsunami propagation when influenced by obstacles (Fig.
 263 1A - white arrow) or not (Fig. 1A - black arrow), respectively and 2) the gradual
 264 disappearance of TT cones toward the unit boundary as compaction, and hence
 265 overpressure, should have decreased as the tsunami wave propagation progressively
 266 lost energy and material while moving 'landward'.



267

268

269 *Figure 11. Lobes flow direction inferred from mounds alignments as marked by dashed black arrows.*
 270 *Contour lines are 50 meters spaced. They show that flows clearly go upslope. g18_025425_2271;*
 271 *b18_016498_2264. Inset: Thumbprint terrain flow exceeding valley scarp (dashed red line) for several*
 272 *kilometers. Unit limit is marked by the red dashed line. The lobe has no peripheral ridges and its front is*
 273 *lobate (HiRISE ESP_016498_2265).*

274 On Earth, geophysical surveys and studies - across the continental margins of the Arctic
 275 Ocean – continuously detect suites of hectometre/meter-wide seafloor mounds

276 accompanied with seepage due to the destabilization of gas hydrates (methane)
277 trapped in seafloor and permafrost-associated sediments (Serov et al., 2015, 2017;
278 Andreassen et al., 2017). Pressure is increased by released methane and triggers
279 blowouts through weakened zones. The Holocene marine transgression affected the
280 Arctic shelves and led to an extensive permafrost thawing; this is the reason why gas
281 hydrate degradation occurs primarily on the circum-Arctic Ocean continental shelves
282 (Macdonald, 1990; Lachenbruch, 1994; Maslin, 2010), where subsea permafrost
283 thawing and methane hydrate dissociation have been triggered by warming and
284 inundation since the Late Pleistocene. Seafloor mounds are steep-sided, up to 1100 m
285 wide, generally semi-circular to elliptical in plan view, and have an irregular upper
286 surface incised with straight or curved furrows. Since the mounds are elevated well
287 above the surrounding seafloor, the most plausible formation mechanism is either
288 deposition or uplift. However, the absence of any discernible seismic paleo-seafloor
289 favours the former hypothesis (Andreassen et al., 2017). We find it difficult to attribute
290 thumbprint terrain cones in Acidalia Planitia to these terrestrial shallow-water sea-
291 mounds considering the scale, mutual geographic distribution, timing of formation and
292 their absence in any terrestrial tsunami deposit since these Martian cones are smaller
293 and more densely coalesced (whether organized or not) than Earth's features.
294 Therefore, TT mounds/cones are more likely thought as mud-volcanoes related to a
295 catastrophic event (tsunami) rather than a release of pressure that gradually
296 accumulated in the sub-surface due to sediment deposition. However, these terrestrial
297 gas blowouts cannot be ruled out for elliptical domes that have been observed outside
298 or under the thumbprint terrain unit (Fig. 2; Fig. 9) and must be further investigated to fit
299 the Acidalia Planitia thumbprint terrain and tsunami-related deposit. The same
300 qualitative thermal inertia response to daily temperature changes between elliptical
301 domes and thumbprint terrain mounds indicates that: 1) these features might be
302 composed by the same material reflecting the uniformity of lithologies in Acidalia
303 Planitia and 2) both elliptical domes and high albedo mound thumbprint terrain
304 alignments are qualitatively finer grained or more poorly consolidated than surrounding
305 areas. This behaviour fits well with average DATI values and conclusion (see section 4).
306 Therefore, elliptical domes may be the result of material extrusion (due to gradual
307 freezing and/or the load of top debris) prior to the extensive viscous flowing (tsunami
308 event) that led to the thumbprint terrain unit overlapping them and making dome
309 detection difficult inside the lobate TT unit.

310 New findings stated that some TT is too young to have experienced the ocean floor
311 environment, and, hence, a tsunami event, according to the current understanding of
312 the cryosphere depth and thermo-chemical structure of Mars (De Toffoli et al., 2019).
313 However, some areas of thumbprint terrain may be old enough to have experienced
314 tsunamis. In De Toffoli et al., 2019, 370 Ma may be the age of a possible ice-rich mantle
315 covering the older underlying TT deposit as it was observed in northern Arabia Terra
316 where a similar thumbprint terrain is covered by young ice-rich ejecta from Lyot crater
317 (48°33'42.72"N 18°12'46.78"E). Moreover, when dating surfaces and bedforms, it has
318 been observed that the floor ages of some Martian outflow channels generally equate to
319 younger mesoscale flows (several hundred meters to a few kilometers) instead of those
320 published in more general geologic maps reflecting older and regional scale processes
321 (Rodriguez et al., 2015). If alignments of cones in Acidalia Planitia were as recent as
322 those analysed in Arcadia Planitia (De Toffoli et al., 2019), their strict occurrence with
323 lobate flow deposits direction and highly organized patterns around obstacles (hills or
324 residual plateaus), matching a very older and distinct tsunami event flow, would be an
325 unusually fortunate coincidence. Consequently, this firmly underlines the importance of
326 investigating thumbprint terrain found in other areas of Mars. High-resolution images
327 may further distinguish multiple TT sets: i) analysing adjacent deposits and the
328 geological context in which they are formed, ii) evaluating origin and/or putative trigger
329 mechanisms discerning any morphological convergence.

330 The ocean hypothesis remains controversial and explanations have been put forward to
331 account for the presence of the TT in the absence of an ocean. For example, Skinner et
332 al. (2008) proposed that the propagation of seismic surface waves through northern
333 plains sedimentary units could have triggered liquefaction and run-up flows along the
334 margins of these deposits. In conclusion, given the morphology, the scale, the thermal
335 inertia analysis, the strict occurrence of thumbprint terrain within lobate deposits and
336 their congruous spatial arrangement with inferred lobes direction, and the significant
337 energy required to surmount little slopes, here we favour a tsunami-related origin for TT
338 in Acidalia Planitia, rather than simply a mud-volcanism deposit.

339

340 **6 Conclusions**

341 This paper renewed questions about the presence of a large standing body of water on
342 Mars by analysing thumbprint terrain, lobate morphologies and deposits in southeastern

343 Acidalia Planitia. The most likely hypothesis is a tsunami-related origin, as lobate TT
344 unit characteristics (e.g., viscosity, onslope flows, etc...), geological setting and numeric
345 simulations are comparable to terrestrial tsunami deposits. Lobate deposits inside
346 valleys, peripheral lobes and lateral ridges, as well as the energy required to surmount
347 little slopes, overlap valley walls and reach the plateau, fit well with a viscous flow of fine
348 material from the advance of a tsunami. Here, we interpret that these lobes are the
349 remnant of an impact-induced flow with high energy that produced a large inundation
350 subsequent to one or several tsunamis. In this context, thumbprint terrain would be
351 related to the final stage evolution of the tsunami wave propagation, i.e. mud volcanoes
352 that extruded water-mud mix material along the tsunami wave fronts. A wider coverage
353 of high-resolution data would improve our understanding and reveal new crucial
354 information in the ongoing debate of thumbprint terrain origin.

355 The presence (Parker et al., 1989, 1993; Head et al., 1998, 1999; Clifford and Parker,
356 2001; Carr and Head, 2003; Tanaka et al., 2003, 2005), and eventual freezing (Ivanov
357 et al., 2014), of a former northern body of water, or a mud-ocean as Jöns (1987)
358 proposed, provides the geological context for thumbprint terrain as mud volcanoes
359 related to a tsunami event. In addition, crater counting showed that lobate TT unit is
360 Early Amazonian; 2.8 ± 0.2 Gyr according to Hartmann 2004-iteration (Fig. S4 -
361 supplementary files). This crater counting analysis is concordant to a crater-retention
362 age of 2.9 Gyr, proposed by Costard et al., 2017 for the same area, and to other
363 previous literature (Hiesinger et al. 2009) which corresponds to an Early
364 Amazonian/Late Hesperian ocean, in agreement with Parker et al., 1993. The Late
365 Hesperian is also the timing of peak outflow channel activity, and thus is consistent with
366 the presence of a transient northern ocean ~3 Ga.

367 Giving morphologies and scales, fully thermal inertia and albedo values compliance,
368 multiple impact craters possibility fitting numerical simulations, the occurrence of TT
369 with lobes, their congruous alignments with inferred lobes direction and in favour of a
370 general geological context, we herein mainly support the tsunami-driven mud-volcanoes
371 hypothesis rather than others mentioned above.

372 **Acknowledgements**

373 This research was partially conducted and supported by the Programme National de
374 Planétologie (PNP) of Institut National des Sciences de l'Univers (CNRS-INSU), the
375 Centre National d'Etudes Spatiales (CNES). The EXOMHYDR project within the TEAM

376 programme of the Foundation for Polish Science co-financed by the European Union
377 under the European Regional Development Fund (contract TEAM/2016-3/20). Our
378 gratitude also goes to Dr. Jakub Ciazela for contribution in the ATI method and
379 estimation of ATI errors. A special thanks goes to Professor Lucia Marinangeli who
380 supported us actively and made it possible to conclude the study.

381

382 **References**

- 383 Andreassen, K., Hubbard, A., Winsborrow, M., Patton, H., Vadakkepuliambatta, S., Plaza-Faverola, A.,
384 ... & Mienert, J., 2017. Massive blow-out craters formed by hydrate-controlled methane expulsion
385 from the Arctic seafloor. *Science*, 356(6341), 948-953.
- 386 Baker, V. R., Strom, R. G., Gulick, V. C., Kargel, J. S., Komatsu, G., Kale, V. S., 1991. Ancient Oceans,
387 Ice Sheets and the Hydrological Cycle on Mars. *Nature*. 352, 589-594.
- 388 Bamberg, M., Asche, H., Jaumann, R., 2013. Additional tools for surface analysis in ArcGIS. EPSC
389 Abstracts Vol. 8, EPSC2013-435, 2013. European Planetary Science Congress 2013.
- 390 Bryant, E. A., 2001. *Tsunami: The Underrated Hazard*, pp. 320, Cambridge Univ. Press, Cambridge.
- 391 Buczkowski, D. L., Cooke, M. L., 2004. Formation of double-ring circular grabens due to volumetric
392 compaction over buried impact craters: Implications for thickness and nature of cover material in
393 Utopia Planitia, Mars. *Journal of Geophysical Research: Planets*. 109.
- 394 Buczkowski, D. L., Seelos, K. D., Cooke, M. L., 2012. Giant polygons and circular graben in western
395 Utopia basin, Mars: Exploring possible formation mechanisms. *Journal of Geophysical Research-
396 Planets*. 117.
- 397 Catling, C., Leovy, C.B., Wood, S.E., Day, M.D., 2012. Does the Vastitas Borealis Formation contain
398 oceanic or volcanic deposits?: Third Conference on Early Mars: Geologic, Hydrologic, and Climatic
399 Evolution and the Implications for Life, 21–25 May 2012, Lake Tahoe, Nevada: LPI Contribution no.
400 1680, abstract 7031.
- 401 Carr, M.H., 1979. Formation of martian flood features by release of water from confined aquifers. *J.
402 Geophys. Res.* 84, 2995–3007.
- 403 Carr, M. H., 1986. Mars - a Water-Rich Planet. *Icarus*. 68, 187-216.
- 404 Carr, M. H., 1990. D/H on Mars Effects of Floods, Volcanism, Impacts, and Polar Processes. *Icarus*. 87,
405 210-227.
- 406 Carr, M.H., 1995. The Martian drainage system and the origin of valley networks and fretted channels.
407 *Journal of Geophysical Research: Planets*, 100(E4), pp.7479-7507.
- 408 Carr, M. H., Head, J. W., 2003. Oceans on Mars: An assessment of the observational evidence and
409 possible fate. *Journal of Geophysical Research-Planets*. 108.
- 410 Christensen, P. R., Jakosky, B. M., Kieffer, H. H., Malin, M. C., McSween, H. Y., Nealon, K., ... & Ravine,
411 M., 2004. The thermal emission imaging system (THEMIS) for the Mars 2001 Odyssey Mission.
412 *Space Science Reviews*, 110(1-2), 85-130.
- 413 Citron, R., Manga, M. & Hemingway, D., 2018. Timing of oceans on Mars from shoreline deformation.
414 *Nature* 555, 643–646 doi:10.1038/nature26144
- 415 Clifford, S. M., Parker, T. J., 2001. The evolution of the Martian hydrosphere: Implications for the fate of a
416 primordial ocean and the current state of the northern plains. *Icarus*. 154, 40-79.
- 417 Cooke, M., Islam, F., McGill, G., 2011. Basement controls on the scale of giant polygons in Utopia
418 Planitia, Mars. *Journal of Geophysical Research-Planets*. 116.

- 419 Costard, F., Séjourné, A., Lagain, A., Ormö, J., Rodriguez, J. A. P., Clifford, S., et al., 2019. The
420 Lomonosov crater impact event: A possible mega-tsunami source on Mars. *Journal of Geophysical*
421 *Research: Planets*, 124, 1840–1851. <https://doi.org/10.1029/2019JE006008>.
- 422 Costard, F., Séjourné, A., Kelfoun, K., Clifford, S., Lavigne, F., Di Pietro, I., Bouley, S., 2017. Modeling
423 tsunami propagation and the emplacement of thumbprint terrain in an early Mars ocean, *Journal of*
424 *Geophysical Research-Planets*. 122.
- 425 De Toffoli, B., Pozzobon, R., Massironi, M., Mazzarini, F., Conway, S., & Cremonese, G., 2019. Surface
426 Expressions of Subsurface Sediment Mobilization Rooted into a Gas Hydrate-Rich Cryosphere on
427 Mars. *Scientific reports*, 9(1), 8603. doi:10.1038/s41598-019-45057-7.
- 428 Farmer, C. B., Doms, P. E., 1979. Global seasonal variation of water vapor on Mars and the implications
429 for permafrost. *J. Geophys. Res.* 84, 2881–2888.
- 430 Farrand, W.H., Gaddis, L. R. , 2003. THEMIS Observations of Pitted Cones in Acidalia Planitia and
431 Cydonia Mensae, Sixth International Conference on Mars, #3094.
- 432 Farrand, W. H., Gaddis, L. R., Keszthelyi, L., 2005. Pitted cones and domes on Mars: Observations in
433 Acidalia Planitia and Cydonia Mensae using MOC, THEMIS, and TES data. *Journal of Geophysical*
434 *Research-Planets*. 110.
- 435 Fergason, R. L., Christensen, P. R., Kieffer, H. H., 2006. High-resolution thermal inertia derived from the
436 Thermal Emission Imaging System (THEMIS): Thermal model and applications. *Journal of*
437 *Geophysical Research-Planets*. 111.
- 438 Frey, J. V., Jarosewich, M., 1982. Subkilometer Martian volcanoes: Properties and possible terrestrial
439 analogs, *J. Geophys. Res.*, 87(B12),9867–9879, doi:10.1029/JB087iB12p09867.
- 440 Greeley, R., Guest, J.E., 1987. Geologic map of the eastern equatorial region of Mars, 1:15,000,000
441 scale. US Geological Survey Geol. Inv. Ser., Map I-1802-B.
- 442 Grizzaffi, P., Schultz, P. H., 1989. Isidis Basin - Site of Ancient Volatile-Rich Debris Layer. *Icarus*. 77,
443 358-381.
- 444 Hartmann, W.K. and Neukum, G., 2001. Cratering chronology and the evolution of Mars. In *Chronology*
445 *and evolution of Mars* (pp. 165-194). Springer, Dordrecht.
- 446 Head, J. W., Hiesinger, H., Ivanov, M. A., Kreslavsky, M. A., Pratt, S., Thomson, B. J., 1999. Possible
447 ancient oceans on Mars: Evidence from Mars Orbiter Laser Altimeter data. *Science*. 286, 2134-
448 2137.
- 449 Head, J. W., et al., 1998. Oceans in the past history of Mars: Tests for their presence using Mars Orbiter
450 Laser Altimeter (MOLA) data. *Geophysical Research Letters*. 25, 4401-4404.
- 451 Heipke, C., Oberst, J., Albertze, J., Attwenger, M., P. Dorninger, P., E. Dorrer, Ewe, M., Gehrke, S.,
452 Gwinner, K., Hirschmüller, H., Kim, J.R., Kirk, R.L., Mayer, H., Muller, J.P., Rengarajan, R.,
453 Rentsch, M., Schmidt, R., Scholten, F., Shani, J., Spiegel, M., Wählisch, M., Neukum, G., & the
454 HRSC Co-Investigator Team (2007). Evaluating planetary digital terrain models—The HRSC DTM
455 test, *Planetary and Space Science*, 55 (14), 2173-2191, doi.org/10.1016/j.pss.2007.07.006.
- 456 Hiesinger, H., Rohkamp, D., Sturm, S., Thiessen, F. and Reiss, D., 2009. Thumbprint Terrain in Isidis
457 Planitia, Mars: Geology, Ages, Morphology, and Morphometry. In *EGU General Assembly*
458 *Conference Abstracts* (Vol. 11, p. 7812).
- 459 Jaumann, R., Neukum, G., Behnke, T., Duxbury, T.C., Eichentopf, K., Flohrer, J., Gasselt, S.V., Giese,
460 B., Gwinner, K., Hauber, E. and Hoffmann, H., 2007. The high-resolution stereo camera (HRSC)
461 experiment on Mars Express: Instrument aspects and experiment conduct from interplanetary
462 cruise through the nominal mission. *Planetary and Space Science*, 55(7-8), pp.928-952.
- 463 Jöns, H. P., 1987. Large fossil mud lakes or giant mud sheet floods in Syrtis Major (Isidis Planitia) and
464 Mare Australe. *Mars. Lunar. Planet. Sci.* 18,470-471.
- 465 Iijima, Y., Goto, K., Minoura, K., Komatsu, G. and Imamura, F., 2014. Hydrodynamics of impact-induced
466 tsunami over the Martian ocean. *Planetary and Space Science*, 95, pp.33-44.

- 467 Ivanov, M. A., Hiesinger, H., Erkeling, G., Reiss, D., 2014. Mud volcanism and morphology of impact
468 craters in Utopia Planitia on Mars: Evidence for the ancient ocean. *Icarus*. 228, 121-140.
- 469 Ivanov, M. A., Hiesinger, H., Erkeling, G., Reiss, D., 2015. Evidence for large reservoirs of water/mud in
470 Utopia and Acidalia Planitiae on Mars. *Icarus*. 248, 383-391.
- 471 Kargel, J. S., Baker, V. R., Begét, J. E., Lockwood, J. F., Péwé, T. L., Shaw, J. S., & Strom, R. G., 1995.
472 Evidence of ancient continental glaciation in the Martian northern plains. *Journal of Geophysical*
473 *Research: Planets*, 100(E3), 5351-5368.
- 474 Kargel, J. S., Strom, R. G., 1992. Ancient Glaciation on Mars. *Geology*. 20, 3-7.
- 475 Kneissl, T., van Gasselt, S., & Neukum, G., 2011. Map-projection-independent crater size-frequency
476 determination in GIS environments—New software tool for ArcGIS. *Planetary and Space Science*,
477 59(11-12), 1243-1254.
- 478 Kholodov, V. N., 2002. Mud volcanoes, their distribution, regularities, and genesis: Communication 1.
479 Mud volcanic provinces and morphology of mud volcanoes. *Lithol. Miner. Resour.*, 27, 197– 209.
- 480 Komatsu, G., Okubo, C. H., Wray, J. J., Ojha, L., Cardinale, M., Murana, A., ... & Gallagher, R., 2016.
481 Small edifice features in Chryse Planitia, Mars: assessment of a mud volcano hypothesis. *Icarus*,
482 268, 56-75.
- 483 Kreslavsky, M. A., Head, J. W., 2002. Fate of outflow channel effluents in the northern lowlands of Mars:
484 The Vastitas Borealis Formation as a sublimation residue from frozen ponded bodies of water.
485 *Journal of Geophysical Research-Planets*. 107.
- 486 Lachenbruch, A. H., 1994. Permafrost, the active layer, and changing climate. Washington, DC: US
487 Geological Survey.
- 488 Lavigne, F., Paris, R., Grancher, D., Wassmer, P., Brunstein, D., Vautier, F., ... & Gomez, C., 2009.
489 Reconstruction of tsunami inland propagation on December 26, 2004 in Banda Aceh, Indonesia,
490 through field investigations. *Pure and Applied Geophysics*, 166(1-2), 259-281.
- 491 Lockwood, J. F., Kargel, J. S., Strom, R. B., 1992. Thumbprint Terrain on the Northern Plains: A Glacial
492 Hypothesis. *Abstracts of the Lunar and Planetary Science Conference*, volume 23, page 795.
- 493 Lucchitta, B. K., 1981 . Mars and Earth: Comparison of cold-climate features. *Icarus*, 45, 264–303,
494 doi:10.1016/0019-1035(81)90035-X.
- 495 MacDonald, G. J., 1990. Role of methane clathrates in past and future climates. *Climatic Change*, 16(3),
496 247-281.
- 497 Mackay, J. R., 1973. The growth of pingos, western Arctic coast, Canada, *Can. J. Earth Sci.*, 10, 979–
498 1004.
- 499 MacKay, J. R., 1998. Pingo growth and collapse, Tuktoyaktuk Peninsula area, western arctic coast,
500 Canada: A long-term field study. *Geogr. Phys. Quat.*, 52, 1– 53.
- 501 Malin, M. C., Bell, J. F., Cantor, B. A., Caplinger, M. A., Calvin, W. M., Clancy, R. T., ... & Lee, S. W.,
502 2007. Context camera investigation on board the Mars Reconnaissance Orbiter. *Journal of*
503 *Geophysical Research: Planets*, 112(E5)..
- 504 Malin, M. C., Edgett, K. S., 2001. Mars Global Surveyor Mars Orbiter Camera: Interplanetary cruise
505 through primary mission. *Journal of Geophysical Research-Planets*. 106, 23429-23570.
- 506 Mangold, N., Allemand, P., Duval, P., Geraud, Y., Thomas, P., 2002. Experimental and theoretical
507 deformation of ice-rock mixtures: Implications on rheology and ice content of Martian permafrost.
508 *Planetary and Space Science*. 50, 385-401.
- 509 Maslin, M., Owen, M., Betts, R., Day, S., Dunkley Jones, T., & Ridgwell, A., 2010. Gas hydrates: past and
510 future geohazard? *Philosophical Transactions of the Royal Society A: Mathematical, Physical and*
511 *Engineering Sciences*, 368(1919), 2369-2393.
- 512 McEwen, A. S., Eliason, E. M., Bergstrom, J. W., Bridges, N. T., Hansen, C. J., Delamere, W. A., ... &
513 Kirk, R. L., 2007. Mars reconnaissance orbiter's high resolution imaging science experiment
514 (HiRISE). *Journal of Geophysical Research: Planets*, 112(E5).

- 515 Mcgill, G. E., Hills, L. S., 1992. Origin of Giant Martian Polygons. *Journal of Geophysical Research-*
516 *Planets.* 97, 2633-2647.
- 517 McGowan, E. M., 2011. The Utopia/Isidis overlap: Possible conduit for mud volcanism on Mars. *Icarus.*
518 212, 622-628.
- 519 Miyakawa, K., Tokiwa, T., Murakami, H., 2013. The origin of muddy sand sediments associated with mud
520 volcanism in the Horonobe area of northern Hokkaido, Japan. *Geochemistry Geophysics*
521 *Geosystems.* 14, 4980-4988.
- 522 Neukum, G. and Jaumann, R., 2004. HRSC: the High Resolution Stereo Camera of Mars Express, ESA
523 SP-1240, September 2004.
- 524 Neukum G. 1983. Meteorite bombardment and dating of planetary surfaces. Translation of: Meteoriten
525 bombardement und Datierung planetarer Oberflächen, Tenure Thesis, Ludwig-Maximilians
526 University, Munich, Germany, NASA Technical Memorandum TM-77558, 1–186.
- 527 Oehler, D. Z., Allen, C. C., 2010. Evidence for pervasive mud volcanism in Acidalia Planitia, Mars. *Icarus.*
528 208, 636-657.
- 529 Parker, T. J., Gorsline, D. S., Saunders, R. S., Pieri, D. C., Schneeberger, D. M., 1993. Coastal
530 Geomorphology of the Martian Northern Plains. *Journal of Geophysical Research-Planets.* 98,
531 11061-11078.
- 532 Parker, T. J., Saunders, R. S., Schneeberger, D. M., 1989. Transitional Morphology in West Deuteronilus
533 Mensae, Mars - Implications for Modification of the Lowland Upland Boundary. *Icarus.* 82, 111-145.
- 534 Paris, R., Wassmer, P., Sartohadi, J., Lavigne, F., Barthomeuf, B., Desgages, E., ... & Gomez, C., 2009.
535 Tsunamis as geomorphic crises: lessons from the December 26, 2004 tsunami in Lhok Nga, west
536 Banda Aceh (Sumatra, Indonesia). *Geomorphology*, 104(1-2), 59-72.
- 537 Perron, J. T., Mitrovica, J. X., Manga, M., Matsuyama, I., & Richards, M. A., 2007. Evidence for an
538 ancient martian ocean in the topography of deformed shorelines. *Nature*, 447(7146), 840-843.
- 539 Platz T., Michael G. G., Tanaka K. L., Skinner J. A. Jr., Kneissl T., and Fortezzo C. M. 2013. Crater-
540 based dating of geological units on Mars: Methods and application for the new global geological
541 map. *Icarus* 225:806–827.
- 542 Rossbacher, L.A., Judson, S. , 1981. Ground ice on Mars: Inventory, distribution, and resulting landforms.
543 *Icarus*, 45(1), 39–59, doi:10.1016/0019-1035(81)90005-1.
- 544 Rodriguez, J.A.P., Faire, A.G., Tanaka, K.L., Zarroca, M., Linares, R., Platz, T., Komatsu, G., Miyamoto,
545 H., Kargel, J.S., Yan, J., Gulick, V., Higuchi, K., Baker, V.R., Glines, N., 2016. Tsunami waves
546 extensively resurfaced the shorelines of an early Martian ocean. *Scientific Reports*, 6, 25106-1788.
- 547 Rodriguez, J.A.P., Thomas Platz, Virginia Gulick, Victor R. Baker, Alberto G. Fairén, Jeffrey Kargel,
548 Jianguo Yan, Hideaki Miyamoto, Natalie Glines, 2015. Did the martian outflow channels mostly
549 form during the Amazonian Period?, 2015. *Icarus*, Volume 257, Pages 387-395, ISSN 0019-1035,
550 <https://doi.org/10.1016/j.icarus.2015.04.024>.
- 551 Sabol, D. E., Gillespie, A. R., McDonald, E., and Danilina, I., 2006. Differential Thermal Inertia of
552 Geological Surfaces. In J. A. Sobrino, ed., *Second Recent Advances in Quantitative Remote*
553 *Sensing*, Publicacions de la Universitat de València, Spain, ISBN: 84-370-6533-X ; 978-84-370-
554 6533-5, 193-198.
- 555 Salvatore, M. R., Christensen, P. R., 2014. On the origin of the Vastitas Borealis Formation in Chryse and
556 Acidalia Planitiae, Mars. *Journal of Geophysical Research-Planets.* 119, 2437-2456.
- 557 Scott, D. H., Underwood, J. R., 1991. Mottled Terrain - a Continuing Martian Enigma. *Proceedings of*
558 *Lunar and Planetary Science.* 21, 627-634.
- 559 Scott, D. H., Dohm, J. M., Rice, J. W. Jr., 1995. Map of Mars showing channels and possible paleolake
560 basins. USGS Misc. Inv. Ser. Map I-2461, scale 1:30,000,000.
- 561 Skinner, J.A., Tanaka, K.L. and Ferguson, R., 2008. Evidence for and implications of liquefaction in the
562 Vastitas Borealis Marginal Unit in southern Utopia Planitia, Mars. In *Lunar and Planetary Science*
563 *Conference* (Vol. 39, p. 2418).

- 564 Skinner, J.A. and Fergason, R.L., 2010. Contrasting Flow Events in Chryse and Acidalia Planitiae, Mars,
565 as Determined Through Landform Mapping and Spatial Analyses. In *AGU Fall Meeting Abstracts*.
- 566 Smith, D. E., et al., 2001. Mars Orbiter Laser Altimeter: Experiment summary after the first year of global
567 mapping of Mars. *Journal of Geophysical Research-Planets*. 106, 23689-23722.
- 568 Salese, F., G. Di Achille, A. Neesemann, G. G. Ori, and E. Hauber, 2016. Hydrological and sedimentary
569 analyses of well-preserved paleo fluvial-paleolacustrine systems at Moa Valles, Mars, *J. Geophys.*
570 *Res. Planets*, 121, 194–232, doi:10.1002/2015JE004891.
- 571 Serov, P., Vadakkepuliambatta, S., Mienert, J., Patton, H., Portnov, A., Silyakova, A., ... & Hubbard, A.,
572 2017. Postglacial response of Arctic Ocean gas hydrates to climatic amelioration. *Proceedings of*
573 *the National Academy of Sciences*, 114(24), 6215-6220.
- 574 Serov, P., Portnov, A., Mienert, J., Semenov, P., & Ilatovskaya, P., 2015. Methane release from pingo-like
575 features across the South Kara Sea shelf, an area of thawing offshore permafrost. *Journal of*
576 *Geophysical Research: Earth Surface*, 120(8), 1515-1529.
- 577 Souček, O., Bourgeois, O., Pochat, S., & Guidat, T., 2015. A 3 Ga old polythermal ice sheet in Isidis
578 Planitia, Mars: Dynamics and thermal regime inferred from numerical modeling. *Earth and*
579 *Planetary Science Letters*, 426, 176-190. Tanaka, K. L., 1997. Sedimentary history and mass flow
580 structures of Chryse and Acidalia Planitiae, Mars. *Journal of Geophysical Research-Planets*. 102,
581 4131-4149
- 582 Squyres, S.W., 1978. Martian fretted terrain: Flow of erosional debris. *Icarus*, 34(3), pp.600-613..
- 583 Tanaka, K. L., Scott, D. H., 1987. Geologic map of the polar regions of Mars, 1:15,000,000 scale. US
584 Geological Survey Geol. Inv. Ser., Map I-1802-C.
- 585 Tanaka, K. L., Skinner, J. A., Hare, T. M., Joyal, T., Wenker, A., 2003. Resurfacing history of the northern
586 plains of Mars based on geologic mapping of Mars Global Surveyor data. *Journal of Geophysical*
587 *Research-Planets*. 108.
- 588 Tanaka, K. L., Skinner, J. A., Hare, T. M., 2005. Geologic map of the Northern Plains of Mars. US
589 Geological Survey Sci. Inv, Map 2888.
- 590 Tuckwell, G. W., Lonergan, L., Jolly, R. J. H., 2003. The control of stress history and flaw distribution on
591 the evolution of polygonal fracture networks. *Journal of Structural Geology*. 25, 1241-1250.
- 592 Wentworth, C.K., 1922. A scale of grade and class terms for clastic sediments. *The journal of*
593 *geology*, 30(5), pp.377-392.
- 594 Wohletz, K. M., Sheridan, M .F., 1983. Hydrovolcanic explosions II. Evolution of basaltic tuff rings and tuff
595 cones, *Am. J. Sci.*, 283, 385– 413.
- 596 Wood, C. A., 1979. Monogenetic volcanoes of the terrestrial planets, *Proc. Lunar Planet. Sci. Conf.* 10th,
597 2815–2840.
- 598 Zuber, M. T., 2018. Oceans on Mars formed early. *Nature* 555.7698 (2018): 592-591.
- 599